The northern Gulf of Mexico offshore super basin: Reservoirs, source rocks, seals, traps, and successes

John W. Snedden, Robert C. Cunningham, and Jon W. Virdell

ABSTRACT

The northern Gulf of Mexico federal offshore area easily qualifies as a super basin based upon estimated petroleum endowment of more than 100 BOE and cumulative production of 60 BOE. Like other super basins, it has multiple petroleum systems and stacked reservoirs. Examination of four key elements of these petroleum systems (reservoirs, source rocks, seals, and traps) yields important insights to the geologic processes that result in such an exceptional habitat for conventional hydrocarbons.

The bulk of hydrocarbon resources in federal offshore waters is in Cenozoic sandstone reservoirs such as the Paleogene Wilcox reservoir of deep-water subsalt areas. Overall, Cenozoic sandstone reservoirs in both suprasalt and subsalt fields yield the highest flow rates and cumulative production volumes. Notable is the recent addition of the deep-water Jurassic Norphlet sandstone play, the newest and second largest by ultimately technically recoverable resources. Overall, Gulf of Mexico reservoirs are diverse, formed in paleoenvironments ranging from aeolian to deep water.

Powering this super basin are three primary marine source rocks centered in the Oxfordian, Tithonian, and Cenomanian–Turonian Stages. These source rock intervals commonly act as top seals, but other Neogene and Mesozoic shales and even carbonate mudstones are also important trap-sealing elements, as proven by analytical work and downhole pressure measurements. The extensive salt distribution and relatively late Cenozoic burial delayed source rock maturation and migration until the culmination of trap formation in many areas.

High rates of Cenozoic deposition on a mobile salt substrate also generated a myriad of salt tectonic structures, ranging from simple diapiric closures and extensional fault traps to complex

Manuscript received April 11, 2020; provisional acceptance May 11, 2020; revised manuscript received June 24, 2020; final acceptance July 14, 2020.
DOI:10.1306/09092020054

AUTHORS

JOHN W. SNEDDEN ~ *Institute for Geophysics, The University of Texas at Austin, Austin, Texas; jsnedden@ig.utexas.edu*

John W. Snedden is a senior research scientist at the Institute for Geophysics, The University of Texas at Austin. He is director of the Gulf of Mexico Basin Depositional Synthesis project, a consortium dedicated to research on the depositional history of the Gulf of Mexico. Prior to taking his current position, he worked in the oil industry for 25 years, exploring basins around the world. He and William Galloway are authors of the recent book, *The Gulf of Mexico Sedimentary Basin: Depositional Evolution and Petroleum Applications* (Cambridge University Press, 2019).

ROBERT C. CUNNINGHAM ~ *ChargeSearch, Llano, Texas; rcunningham.cs@gmail.com*

Robert C. Cunningham is a petroleum systems consultant with a primary focus on analyzing and mapping source properties in conventional and unconventional plays. In his 31 years in the oil industry, he led teams on global source rock prediction and basin modeling and conducted petroleum systems analysis in basins throughout the world.

JON W. VIRDELL ~ *Institute for Geophysics, The University of Texas at Austin, Austin, Texas; jvirdell@ig.utexas.edu*

Jonathan W. Virdell is a project manager at the Institute for Geophysics, The University of Texas at Austin. He is part of the Gulf of Mexico Basin Depositional Synthesis project research team, contributing his experience in geographic information systems and geophysical data. He holds an A.S. in environmental science and technology from Austin Community College and a B.A. in biology from The University of Texas at Austin.

ACKNOWLEDGMENTS

The authors would like to acknowledge support of the Industrial Associate members of the Gulf of Mexico Basin Depositional Synthesis project at The University of Texas at Austin. We also appreciate discussions with and contributions from the following

individuals: William Galloway, Thomas Ewing, Andrew Pepper, Tony Dupont, Paul Weimer, Michael Hudec, Mark Rowan, Tim Whiteaker, Brad Prather, and Charles Sternbach. Ted Godo is thanked for his permission to use several figures from his seminal 2019 paper on the Norphlet deep-water play and related discussions. We also appreciate GeoMark Research Ltd. and TDI-Brooks International Inc. for providing Robert C. Cunningham with prior access to their seep and reservoir oil geochemical database. We also acknowledge access to Gulf-wide seismic data by ION and Spectrum.

subsalt configurations such as salt-cored compressional anticlines, salt-cutoff traps, and bucket weld traps. Exploration success in the past 20 yr is a direct result of improved seismic imaging around and below salt, as well as advances in drilling, completing, and producing wells and fields.

INTRODUCTION

Overview

The concept of a "super basin" is relatively new, first coined by Fryklund and Stark (2016), who defined it as a basin having a prolific petroleum system (remaining recoverable reserves >5 BOE; past production >5 BOE), a well-established surface infrastructure, ready access to markets, multiple petroleum systems, and stacked reservoirs.

With an estimated endowment of 112.8 BOE of ultimate technically recoverable resources (UTRR) and cumulative production of 60 BOE (Bureau of Ocean Energy Management, 2017; Duncan et al., 2018), the offshore United States or northern Gulf of Mexico (GOM) Basin easily qualifies (Figure 1). In fact, more than 50% of the estimated UTRR in the United States as a whole are situated in the northern GOM (US Geological Survey, 2005).

Past production exceeding five BOE is another threshold that super basins must exceed according to the definition from Fryklund and Stark (2016). This often requires wells with high flow rates, particularly in deep-water areas where costs of development and production are extraordinarily high. For example, the top 10 producing wells in the northern GOM by both average production rate (Figure 2A) and cumulative production (Figure 2B) are all located in deep-water areas and are largely relatively young (Pliocene and Miocene) sandstones whose porosity and permeability are high (>20% porosity, a darcy or more of permeability; Hentz et al., 1997; Weimer et al., 1998). Notable exceptions are wells at St. Malo and Chinook that are older Paleogene-age Wilcox reservoirs (Weimer et al., 2016b) that benefit from novel completion and stimulation techniques such as "frac packs" (Mattos et al., 2013).

Other criteria for a super basin are the presence of a well-established production infrastructure and ready access to markets for commodities (Fryklund and Stark, 2016). In the northern GOM federal waters (beyond the 5-mi [8-km] state limit), it is estimated that more than 7000 drilling and production platforms have been installed. More than 52,000 wells have been drilled offshore at the time of this writing. Fields have been discovered in both state waters and onshore in trends extending north from the United States–Mexico border to the southern tip of Florida.

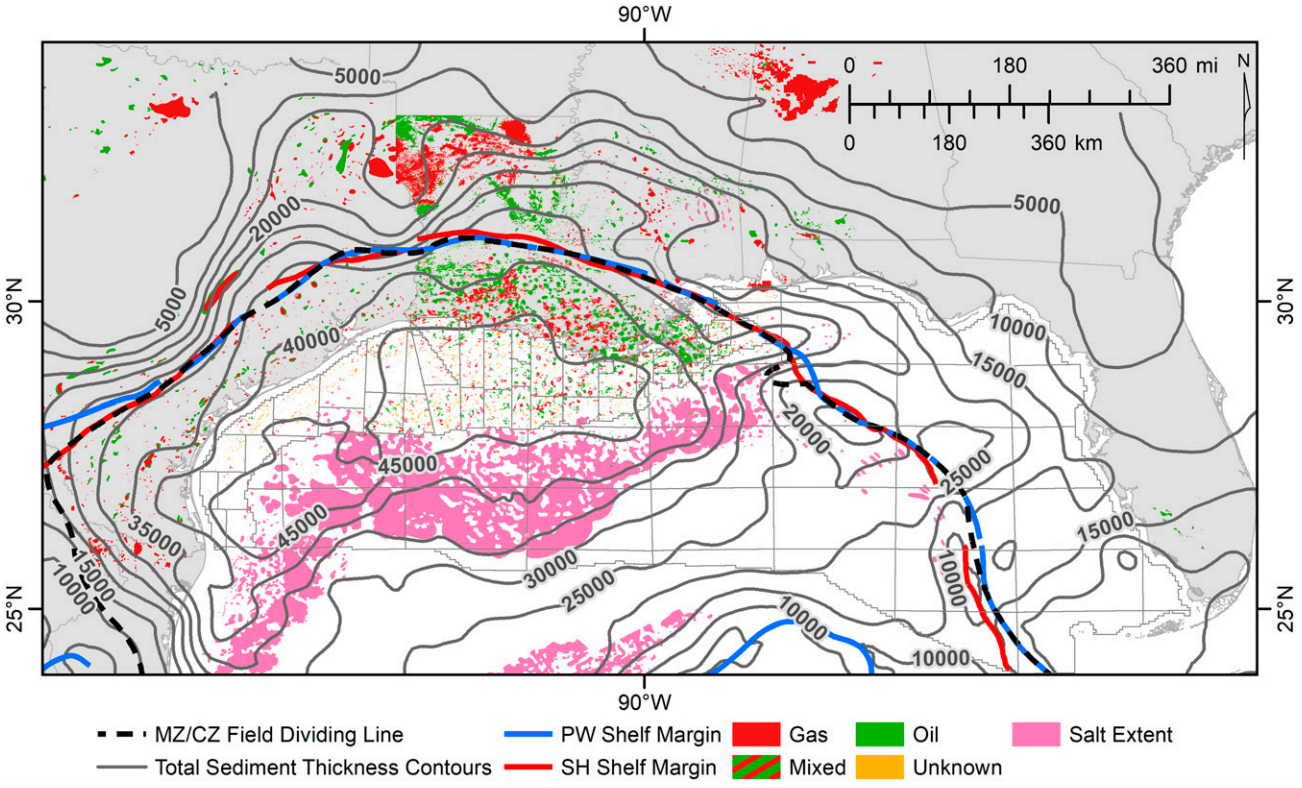

Figure 1. Location map of the United States (northern) Gulf of Mexico Super Basin as defined here. The dashed line separates Mesozoic (MZ) fields and discoveries on the north from Cenozoic (CZ) fields and discoveries located basinward. Data from Bureau of Ocean Energy Management (2017) and US Geological Survey (2005). PW = Paluxy–Washita supersequence; SH = Sligo–Hosston supersequence.

The geologic factors that distinguish super basins from other global basins are somewhat less quantitative. Super basins are often described as including multiple source rocks charging numerous stacked reservoirs (Fryklund and Stark, 2016). Despite the prolific GOM Basin hydrocarbon production and remaining potential reserves, few recent papers have attempted to compile, synthesize, and illuminate this super basin's key success factors in a single document.

The purpose of this paper is to describe in summary fashion the four key elements of the GOM Basin that have powered the enormous hydrocarbon endowment that put this area in the top tier of petroleum habitats. Examples of key reservoirs, source rocks (and maturation windows), seal rocks, and traps are provided. We focus our discussion on regional to basin-wide trends and do not delve into block- or prospect-specific controls such as local burial or hydrocarbon charge history or individual salt tectonic structures.

Several super basins have both conventional and unconventional plays, sometimes linked to the same petroleum system. As described later in this paper, at least two major source rocks (Tithonian centered and Cenomanian–Turonian) are present basin-wide, charging offshore conventional traps but also acting as continuous resources for onshore unconventional plays. Our discussion here, however, is limited to the offshore conventional plays that dominate the current UTRR. The reader is referred to several other publications that describe unconventional plays in the GOM Basin, including Hammes et al. (2011, 2016), Enomoto et al. (2012), Hackley (2012a, b), and Snedden and Galloway (2019).

Geographic Location of Basin, Fields, and Discoveries

The GOM Basin as a whole surrounds and includes a large body of water connected to the Atlantic Ocean via the Straits of Florida (Figure 1). In United States waters, it extends north from the deep abyssal plains in its center to its termination south of the largely

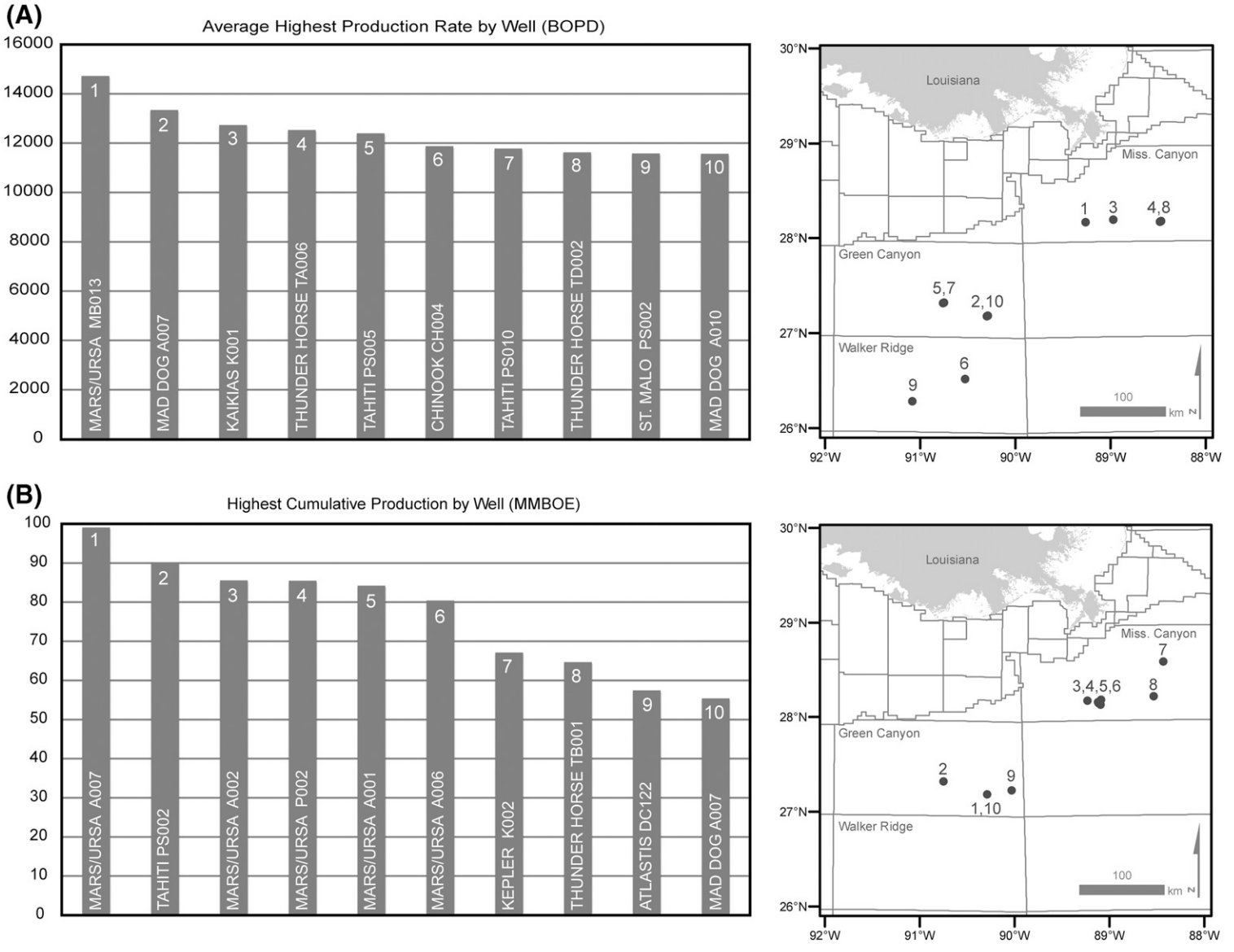

Figure 2. Top 10 wells by average production rate (A) and cumulative production (B) in the northern Gulf of Mexico. All are located in the deep-water area of the northern Gulf of Mexico, specifically in the Green Canyon, Mississippi (Miss.) Canyon, and Walker Ridge Protraction blocks (location map). Here, subsurface pressures (>15,000 psi) and reservoir permeabilities are very high (commonly >100–1000 md), yielding very high flow rates. Most are Miocene- to Pliocene-age sandstone reservoirs with the exception of two Paleogene-age reservoirs in the Chinook and St. Malo fields. Data compiled by Earth Science Associates (courtesy of T. Dupont) from Bureau of Ocean Energy Management released reports.

buried Paleozoic Ouachita thrust belt and east to the Straits of Florida connection with the Atlantic Ocean.

Hydrocarbon discoveries and continuous resource plays in the northern GOM Basin occur in an arcuate trend (Figure 1). With few exceptions, a dividing line can be drawn between carbonate-dominated, largely onshore Mesozoic fields and discoveries and that of the siliciclastic-prone Cenozoic hydrocarbon habitat. This dashed line coincides with the downdip limit of Mesozoic platform margin reefs, largely pinned by a major increase in accommodation at a deep crustal boundary. Cenozoic systems, by contrast, backed by large sediment influxes sourced by the United States Cordilleran and Laramide tectonic belts, prograded past this line in an attempt to fill this basin center.

Despite continuous exploration of this basin since the discovery of oil at the Spindletop salt dome near the turn of the twentieth century, there remains large white spaces with no current hydrocarbon fields or past discoveries. Some areas are restricted by drilling moratoria, such as the Florida shelf and adjacent deep water. In other areas, deep Cenozoic burial and/or challenges to imaging below the modern salt canopy hampered exploration until recently developed techniques like wide-azimuth seismic acquisition were employed (as discussed in later sections).

GEOLOGIC HISTORY

Mesozoic Tectono-Stratigraphic Phases

Comprehensive synthesis of the GOM Basin history, in light of new scientific and exploration insights, is described in detail in Snedden and Galloway (2019), which we summarize briefly here. The tectono-stratigraphic system encompasses six phases, three each in the Mesozoic and Cenozoic Eras (Figure 3). These phases reflect both the long-term tectonic evolution of the basin and its predecessors, as well as the shorter-term eustatic and climatic processes influencing sedimentation. Although the Cenozoic phases have higher frequency (four phases over 66 m.y.), one can argue for three Mesozoic tectono-stratigraphic phases over 170 m.y. or more since the end of the suturing of Pangea and joining of Laurentia and Gondwana. The three phases that cover the post-Ouachita–Marathon–Appalachian orogeny to the end of the Cretaceous (299–66 Ma) are the postorogenic successor basin-fill and rifting phase, the Middle Mesozoic drift and cooling phase, and the Late Mesozoic local tectonic and crustal heating phase.

We regard the first phase as a predecessor to formation of the GOM Basin, but it is worthwhile to discuss some of the tectonic and stratigraphic elements that persisted into the Middle Mesozoic drift and cooling phase or even later. Galloway (2008) has argued that the GOM Basin initiated with deposition of the Louann Salt, the first stratigraphic unit that spans the nascent GOM. Salt deposition was probably underway at 170 Ma, at the start of the drift and cooling phase (Peel, 2019; Snedden et al., 2019). New plate tectonic models suggest that accelerated opening of the Gulf began as an intrusive phase of oceanic crust generation below the accumulating mass of evaporites and later extrusive separation of salt bodies between the northern and southern GOM (Norton et al., 2016).

During the initial stages of basin opening (Middle Mesozoic and drift and cooling phase), arid climate conditions persisted, and a broad belt of dryland deposition, including a prominent aeolian sand sea (erg), developed in the eastern part of the northern GOM (Mancini et al., 1985; Snedden and Galloway, 2019). The largest Mesozoic reservoir by UTRR in federal waters (Figure 4), the Norphlet play fairway now extends from onshore areas to state waters to the Mississippi Canyon (MC) and Desoto Canyon (DC) protraction blocks in deep water. Smaller dryland systems including aeolian dunes are present in Cuba (San Cayetano Formation) (Haczewski, 1976) and in Mexico where the Bacab Sandstone produces oil in the Ek, Balam, and other fields (Cantú-Chapa, 2009; Snedden et al., 2020). Local restrictions in deep bottom water circulation allowed preservation of organics in both the Oxfordian and Tithonian, forming important source rocks (Hood et al., 2002; Cunningham et al., 2016).

The late Mesozoic local tectonic and crustal heating phase followed the end of seafloor spreading in the GOM. The basin at this point reached its present size, and, combined with favorable climatic conditions, carbonate systems transitioned from local grainstone shoals and thrombolite buildups to platform margin and shelf interior reefs and associated grainstone aprons (Mancini et al., 2004). Siliciclastics from the older source terranes like the Appalachians were largely trapped behind the reef margins, reducing turbidity that would have otherwise limited the

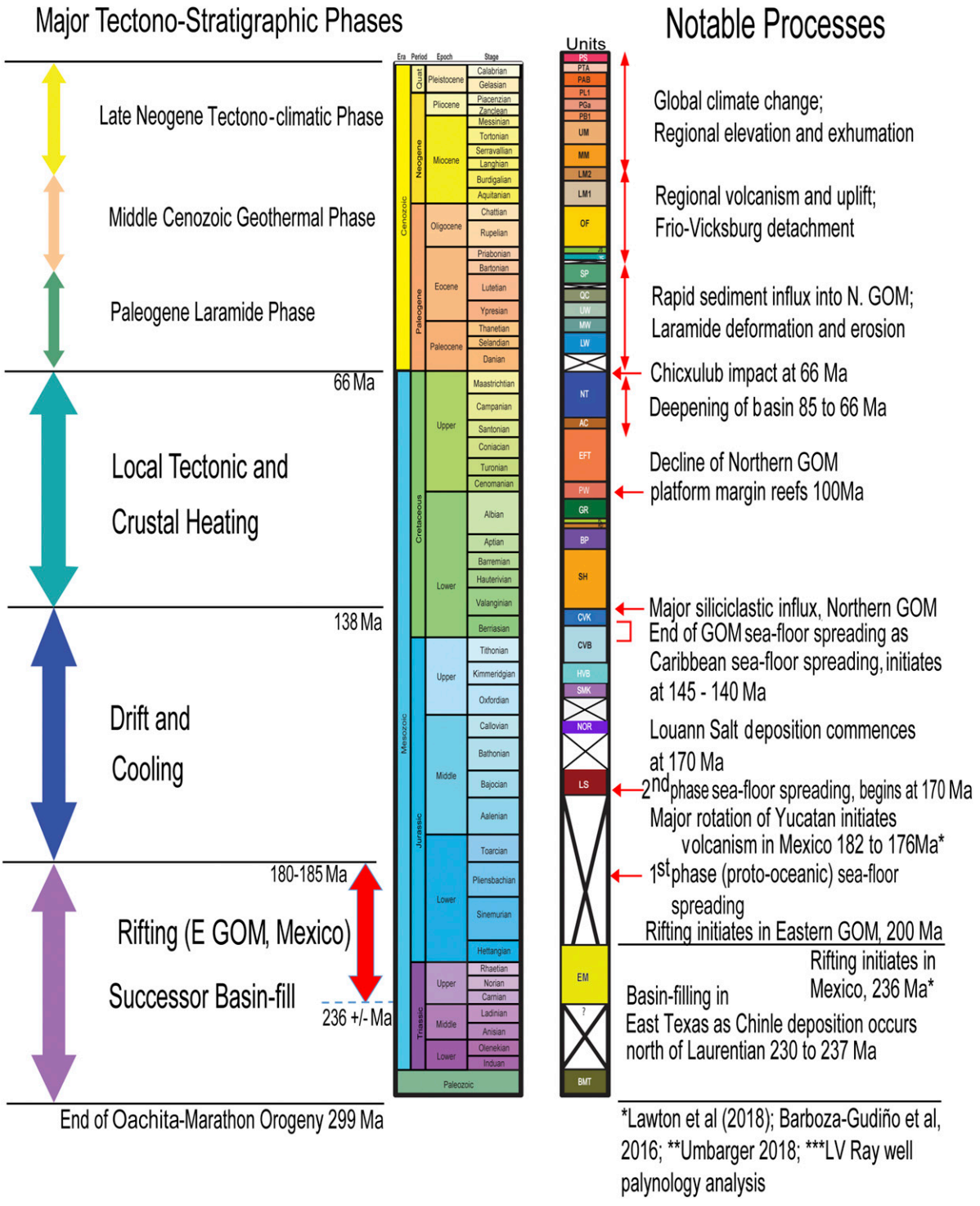

Figure 3. Major tectono-stratigraphic phases, Gulf of Mexico (GOM) Basin, and predecessors. From Snedden and Galloway (2019), courtesy of Cambridge University Press. AC = Austin Chalk; BMT = basement; BP = Bexar–Pine Island Shale; CVB = Cotton Valley–Bossier; CVK = Cotton Valley–Knowles; E = eastern; EFT = Eagle Ford–Tuscaloosa; EM = Eagle Mills; FL = Ferry Lake Anhydrite; GR = Glen Rose; HVB = Haynesville–Buckner; JS = Jackson–Yazoo; LM1 = lower Miocene 1; LM2 = lower Miocene 2; LS = Louann Salt; LW = lower Wilcox; MM = middle Miocene; MW = middle Wilcox; N. = northern; NOR = Norphlet; NT = Navarro–Taylor; OF = Frio–Vicksburg; PAB = Pleistocene-Angulogerina B; PB1 = Miocene–Pliocene-Buliminella 1; PGa = Pliocene-Globigerina altespira; PL1 = Pliocene–Pleistocene-Lenticulina 1; PS = Pleistocene; PTA = Pleistocene–Trimosina A; PW = Paluxy–Washita; QC = Queen City; Quat = Quaternary; RD = Rodessa; SH = Sligo–Hosston; SMK = Smackover; SN = Smackover–Norphlet; SP = Sparta; UM = upper Miocene; UW = upper Wilcox; YC = Yegua–Cockfield.

growth of frame-building corals, sponges, and rudistid bivalves. This reached an acme in the middle Cretaceous (Albian) as reefal systems delineated the basin margin but also surrounded isolated platforms in Mexico. Small but still economically important carbonate reservoirs of the Cretaceous Andrew Formation and James Limestone (Kosters et al., 1989; Petty, 1999) are part of this phase of high carbonate productivity. Igneous activity and uplifts locally developed with igneous intrusive-cored bathymetric highs forming the site of carbonate buildups (Ewing, 2009).

An abrupt termination of reefal carbonate deposition at the end of the Albian has been attributed to several causes, including increased water turbidity with the Tuscaloosa sandstone influx (Snedden et al., 2016), uplift in the Mississippi Embayment (Cox and Van Arsdale, 2002), and the cumulative effects of a series of oceanic anoxic events (OAEs) (Phelps et al., 2015). The OAE2 is associated with development of the Cenomanian–Turonian source rock (Eagle Ford equivalent), although regional conditions such as strong outflow bottom water flow caused a temporal offset from the global event (Lowery et al., 2017). Following the major sand volume influx that built a large Cenomanian–Turonian (Tuscaloosa) submarine fan present in deep water, global sea-level rise flooded the basin. As a result, deep shelf and basinal carbonates including chalks dominated the latest Mesozoic.

The end of the late Mesozoic local tectonic and cooling phase, and the Mesozoic as a whole, was ushered in by the Chicxulub impact event at 66 Ma, which greatly altered the paleobathymetry and land surface of the GOM (Denne et al., 2013; Sanford et al., 2016; Lowery, et al. 2018). It also, to some degree, set up the basin configuration that the Cenozoic tectono-stratigraphic phases modified by sediment input from the newly emerged Laramide highlands and rejuvenated Appalachians mountains (Boettcher and Milliken, 1994; Galloway et al., 2011; Blum and Pecha, 2014; Snedden et al., 2018).

Cenozoic Tectono-Stratigraphic Phases

Much like the Mesozoic fill, the Cenozoic fill of the GOM can be subdivided into three tectono-stratigraphic phases. Unlike Mesozoic phases, they do not reflect processes of basin opening and evolution; rather, they record a combination of influences driven by convergence along the western North American plate margin, by intraplate tectonism, by evolving patterns of continental climate and consequent drainage basin evolution and runoff, and finally by global climate change and resultant glacio-eustasy. Snedden and Galloway (2019) refer to these as the Paleogene Laramide phase, the middle Cenozoic geothermal phase, and the Neogene tectono-climatic phase.

Paleogene Laramide Phase

The structural architecture of the northern GOM at the start of the Cenozoic reflected the far field but still prominent effects of the Chicxulub impact event (Denne et al., 2013). It also inherited the shallow shelf, relict carbonate platform margins, and deep basin configuration of the preceding Cretaceous Period. Laramide deformation in the western United States progressed from north to south, generating a voluminous increase in siliciclastics that quickly filled in Rocky Mountain Basin accommodation. Large trunk rivers flowed toward the northern GOM Basin during a relatively humid climatic phase with vast swamps and wet coastal plains developed in the Paleocene and Eocene (DeCells, 2004; Snedden and Galloway, 2019)

The northern Gulf Paleogene record includes three expanded depositional supersequences: (1) lower Wilcox, (2) middle Wilcox, and (3) upper Wilcox (Galloway et al., 2011). These three major siliciclastic successions include reservoirs formed in the full paleoenvironmental spectrum from bedload–dominated fluvial to abyssal plain fans. Submarine fan run-out lengths in the 1000-km range scaled to the length of the large extrabasinal rivers extending back to the northern Rockies (Snedden et al., 2018). Exploration followed the Wilcox reservoirs from shallow fields onshore to deep-water fields below the salt canopy, transitioning reservoir styles from fluvial to delta or shore zone to slope and submarine fan and commodity type (water, coal, gas, and oil) along the way to the deep basin. The bulk of sedimentation was in the western half of the northern GOM, linked to several continental scale rivers draining the emerging Rockies. Deposited onto salt on its downdip extent, the immense sediment load drove salt evacuation and the seaward and upward migration of the allochthonous salt canopy.

Massive extensional systems generated landward are partially compensated by folding and contraction downdip, with localized shortening and folding of salt. Burial of Mesozoic source rocks initiated hydrocarbon

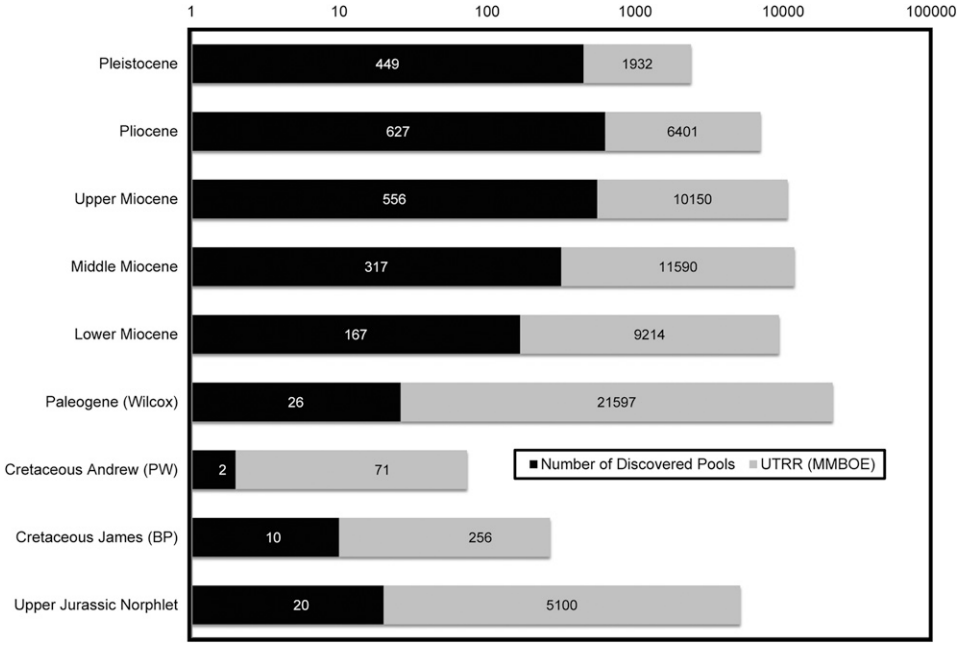

Figure 4. Major northern Gulf of Mexico reservoirs by number of pools (black columns) and total ultimate technically recoverable reserves (UTRR) (gray columns). The 2014 resources from Bureau of Ocean Energy Management (2017). From Snedden and Galloway (2019), courtesy of Cambridge University Press. BP = Bexar–Pine Island supersequence; PW = Paluxy–Washita supersequence.

maturation and migration except below the paleo-canopy where heat flow was much reduced.

Middle Cenozoic Geothermal Phase

The middle Cenozoic geothermal phase is a 23-m.y. record of tectonic reorganization of western North America, as new crustal uplifts and volcanic centers generated new source terranes. Sediment load in the main trunk streams was impacted by volcanic eruptions, particularly in the southwestern sectors where the paleo Rio Grande and other rivers were choked with volcanic ash. The major depositional influx during deposition of the Oligocene Frio supersequence filled accommodation space onshore in the Frio–Vicksburg fault zone, which in combination with more arid climates in the Rockies, constrained sediment bypass to the deep basin. Eastern parts of the basin continued to be relatively sediment starved, a pattern initiated in the Paleogene. Elsewhere, crustal tilting and elevation of the basin fringe amplified normal basinward displacement of both the sediment prism and mobilized salt (Galloway et al., 2011; Snedden and Galloway, 2019).

Late Neogene Tectono-Climatic Phase

The final 15 m.y. of depositional history in the northern GOM records a relative decline in siliciclastic sediment supply from inland source terranes, but it is still notable in size and extent. Rejuvenation of older Appalachian Mountains (caused by deep crustal processes) led to a shift of sedimentation to the eastern areas, culminating in two basin-scale submarine fans as found in the MC, Walker Ridge, and Lund protraction blocks (Galloway, 2008). These form amalgamated reservoir sequences above the salt canopy in load-induced minibasins.

By the Pliocene, competing rivers from the Western Interior and Appalachians first progressively coalesced into three paleo-rivers and then finally into one major river, the forerunner of the modern Mississippi system. Pleistocene glaciation fed immense volumes of sediment to this river, culminating in the Mississippi Fan, which today covers nearly half of the northern GOM Basin (Galloway et al., 2011). Salt-defined minibasins in the western and central deep-water areas continued to fill throughout the Pliocene–Pleistocene and spilled sands basinward and further south past the Sigsbee margin where the allochthonous salt canopy meets the modern seabed (Snedden and Galloway, 2019).

The net result of 66 m.y. of siliciclastic deposition is a super basin whose floor is almost completely covered by long and broad submarine fans of various ages (Figure 5). This in turn reflects the dominance of large river systems fed by an evolving tectonic landscape, favorable climatic conditions, and time-averaged close

proximity of delta point sources to the slope and basin (Sweet and Blum, 2016; Snedden et al., 2018). Wholesale shelf edge bypass, with focused sand transport onto and across the abyssal plain, was a major feature of both greenhouse (Paleocene–early Eocene) and icehouse (Miocene–Pleistocene) worlds (Sweet and Blum, 2011). These basin-scale submarine fans deposited thick successions of stacked reservoirs that when filled by migration of hydrocarbons into salt tectonic traps sealed by deep-water mudstones, they support field sizes ranging up to giant class (Weimer et al., 2017c).

RESERVOIRS

As mentioned previously, the presence of stacked reservoirs is one characteristic of super basins. Conventional reservoirs provide both the storage capacity (often expressed as porous rock volume) and necessary flow capacity (indicated by in situ permeability). Adequate net porous and permeable rock is a prerequisite for commercial development of discoveries. In the GOM, both sandstone and carbonate reservoirs were deposited in a variety of sedimentary settings from nonmarine to deep marine (Ewing and Galloway, 2019).

Virtually every stratigraphic interval above the Louann Salt contains reservoirs that in some part of the greater GOM Basin harbor hydrocarbons, either conventional sandstone or carbonate types or unconventional source rock reservoirs (Snedden and Galloway, 2019). Commercial development of the unconventional resources is limited to onshore areas where the cost of production infrastructure is far lower

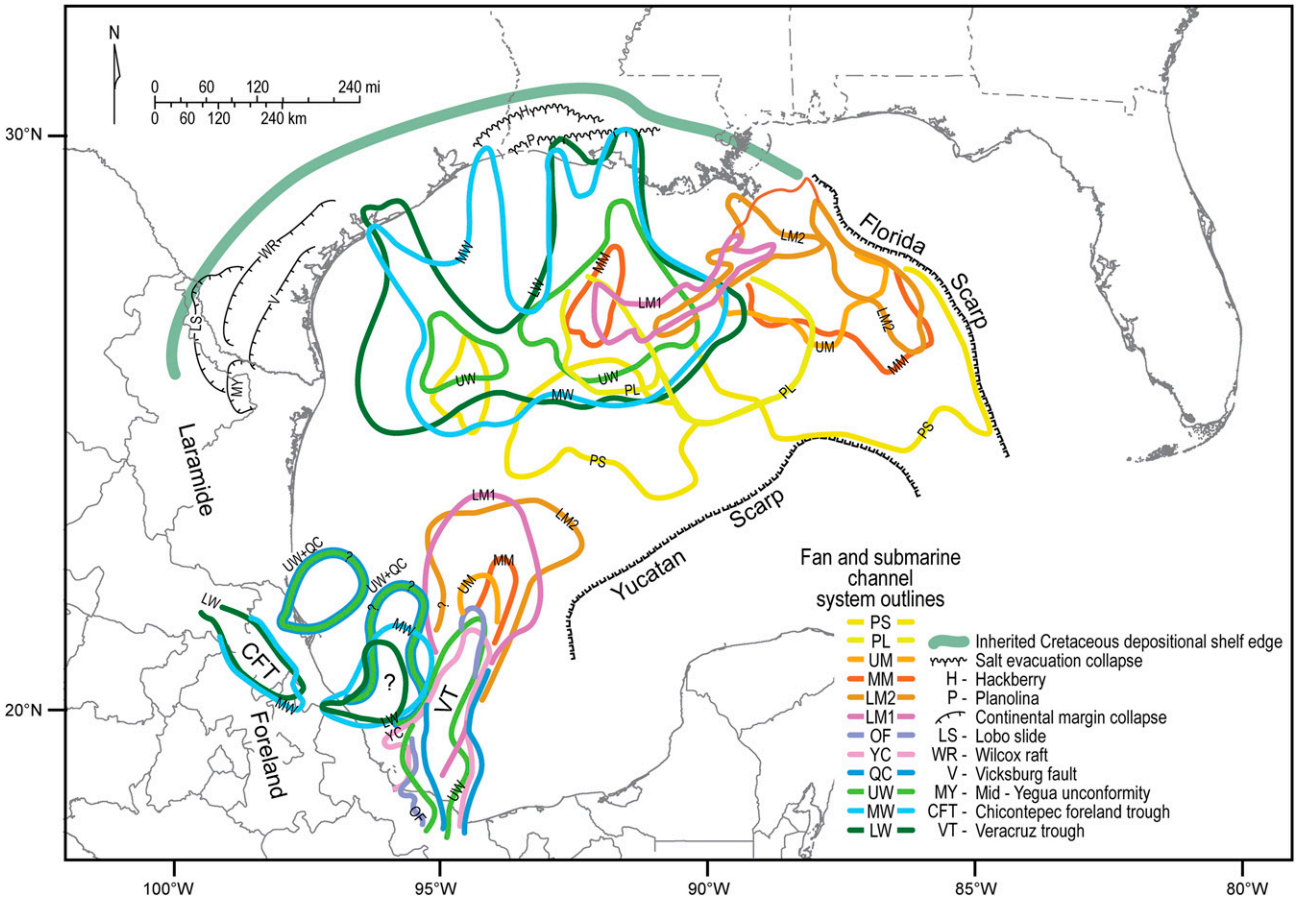

Figure 5. Compiled distribution of (1) collapsed continental margins, (2) submarine channel complexes, and (3) abyssal plain fan systems. The features are collected within boundaries of the Cenozoic deep-water Gulf of Mexico, including the inherited Cretaceous depositional shelf edge, Florida scarp, Campeche scarp, and Laramide foreland. Large submarine fans are concentrated in the northern Gulf of Mexico. Small-to-medium fans and stacked submarine channel complexes occupy the southwest Gulf. From Snedden and Galloway (2019), courtesy of Cambridge University Press. ? = extent of Chicontepec canyon fan is hypothetical; LM1 = lower Miocene 1; LM2 = lower Miocene 2; LW = lower Wilcox; MM = middle Miocene; MW = middle Wilcox; OF = Frio–Vicksburg; PL = Pliocene–Pleistocene-Lenticulina 1; PS = Pleistocene; QC = Queen City; UM = upper Miocene; UW = upper Wilcox; YC = Yegua–Cockfield.

than in the offshore transition zone, shelf, or deep water.

In United States federal offshore waters, however, the vast majority of fields and discoveries are developed in Cenozoic sandstone reservoirs (Figure 4). These reservoirs produce at the highest average rates and historically have the largest cumulative production (Figure 2A, B). This is because of the high porosity and permeability of these relatively young, uncompacted, and diagenetically unaltered quartzose sandstones (Hentz et al., 1997; Marchand et al., 2015).

Of the Cenozoic intervals, all reservoirs are sandstones ranging in age from Paleocene to Pleistocene. The Paleogene (Eocene and Paleocene) Wilcox now hosts the largest UTRR (Bureau of Ocean Energy Management, 2017; Figure 4). The Wilcox deep-water play was ushered in by the drilling of the BAHA II well and subsequent oil discoveries (Zarra, 2007). Success of post-2000 subsalt exploration is evident in the large number of fields and discoveries (26 total). Younger-age reservoirs within the Pliocene and Pleistocene were drilled earlier in the shallower postsalt section, making effective use of seismic facies and amplitudes and regional mapping (Prather et al., 1998). In the eastern GOM, middle and upper Miocene sandstones are the primary reservoirs in giant and supergiant fields like Thunderhorse (Henry et al., 2017; Weimer et al., 2017b, c)

Emerging plays in the inboard subsalt areas of Green Canyon (GC) and Garden Banks (GB) protraction blocks include the middle and lower Miocene reservoirs are found in Tahiti, Holstein Deep, and Vito fields and discoveries (Thacher et al., 2013; Figure 4). The recent Paleogene discovery at Anchor also is located in this same general area (Zarra et al., 2019). Earlier exploration in outboard areas, where the salt canopy is less complex, discovered oil in middle Miocene reservoirs such as in the Atlantis field of the GC protraction block (Mander et al., 2012).

The few Mesozoic exceptions to the Cenozoic dominance of northern GOM offshore production include the Middle Jurassic (Oxfordian) Norphlet Formation, the Cretaceous (Aptian) James Limestone, and Cretaceous (Albian) Andrew Formation (Figure 4). The Norphlet Formation is the largest and newest Mesozoic reservoir and is already one of the largest overall. It differs from most northern GOM Cenozoic producing reservoirs in several ways. First, the sandstones are thought to have formed in a dryland depositional system, which differs from all other reservoirs in present-day deep-water settings of the northern GOM (Figure 6). Many cores from deep-water Norphlet wells show repetitive successions of quartz-rich sandstones with high-angle cross-beds typical of large aeolian dunes (Godo, 2019; Figure 7A). Cross-beds are consistently unimodal with interpreted paleowinds converging around the western end of the Middle Ground arch where the Norphlet thicknesses can exceed 1000 ft (305 m) (Hunt et al., 2017). Our reconstructions depict a long phase of arid climate and strong winds sweeping loose terrigenous sediment off of large exposed continental land masses of the North American and African plates, which were in close proximity prior to the initiation of sea-floor spreading in the Late Jurassic (Snedden and Galloway, 2019). Sandstones accumulated in salt-defined depocenters that varied from aeolian dune to ephemeral stream fluvial deposits (Godo, 2019; Figure 6). The best sandstones are in the aeolian dune deposits because of mitigation of burial diagenesis by the presence of grain-rimming chlorite that resisted quartz cementation in these deeply buried reservoirs (Godo, 2017).

Second, many of the Norphlet oil discoveries reflect raft tectonics, as blocks of Smackover and Norphlet glided down a paleoslope to the west and south from the Middle Ground arch (Pilcher et al., 2014). Thus, reconstructions of this important depositional system require both restoration back to a pre–sea-floor spreading state as well as corrections for raft translation and rotation (Snedden and Galloway, 2019).

Shell's initial discovery was made at the Shiloh prospect (DC 269-1; see location 7 in the Appendix) in 2003, but a 10-yr campaign of acreage bidding and leasing, exploration drilling, and appraisal eventually led to the first Norphlet deep-water development at Appomattox (MC 392 and adjacent blocks; Godo, 2017) that started production in May 2019. Subsequent deep-water Norphlet discoveries at Rydberg (2014), Fort Sumter (2016), and Ballymore (2017) confirm the importance of this play (locations 9, 31, and 27 in Figure 6, respectively, and location information in the Appendix).

The remainder of the Mesozoic UTRR is found in relatively small fields and discoveries in carbonate reservoirs of the shallow eastern GOM shelf. The

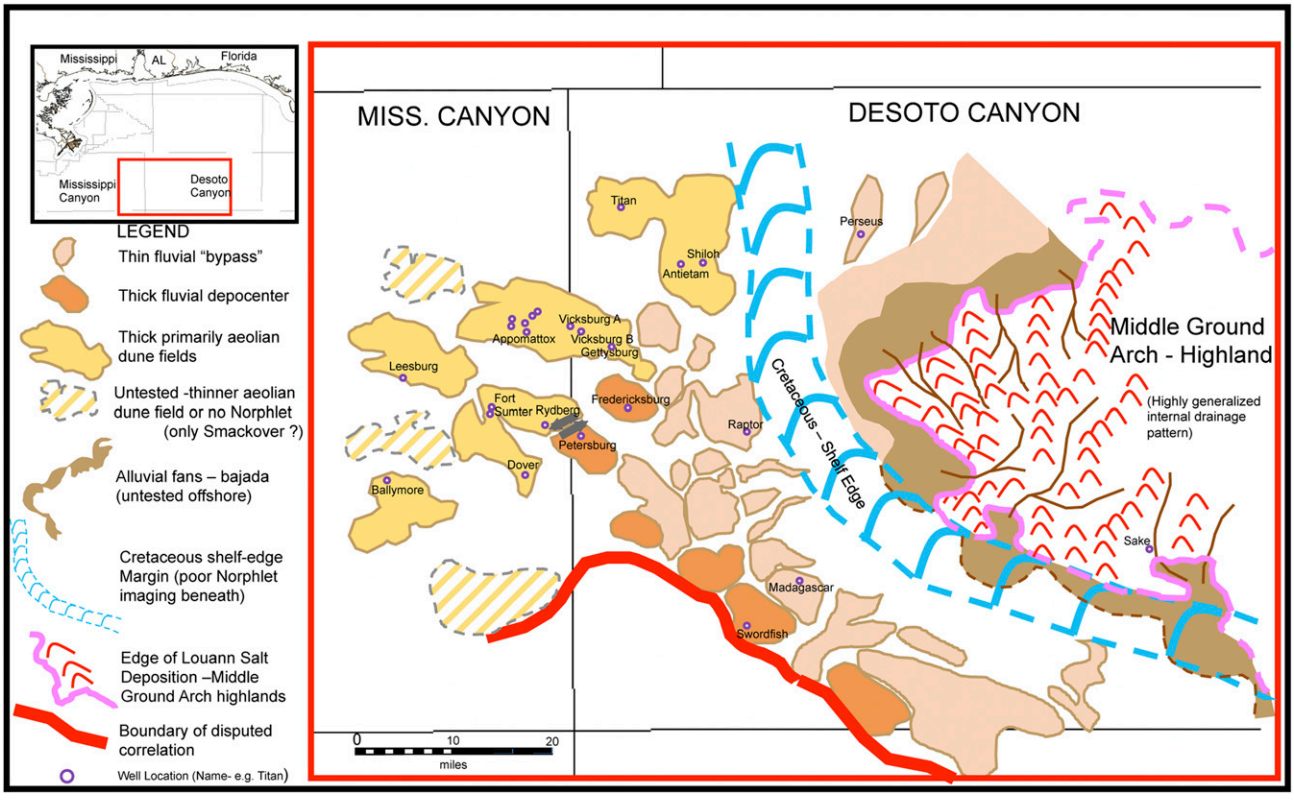

Figure 6. Schematic present-day (unrestored) location of Norphlet dryland systems in the deepwater play area of the eastern Gulf of Mexico. Sandstones accumulated in salt-defined depocenters that vary from confirmed aeolian dune (yellow-colored polygons) to ephemeral stream fluvial deposits (burnt orange colored polygons) and bypass zones (tan-colored fill). Untested depocenters are shown as hachured polygons. White areas between depocenters include salt walls and zones of salt inflation caused by sediment loading at the time of deposition. Approximate well locations are shown. Modified from Godo (2019) and reproduced with permission from the Gulf Coast Association of Geological Societies. AL = Alabama; MISS. = Mississippi.

Andrew and James are carbonate reservoirs, extensions of onshore Mesozoic production to shallow offshore areas (Petty, 1999)

Earlier exploration phases onshore and in shallow waters did cover the full spectrum of siliciclastic reservoir types from fluvial to shore zone, deltaic, and shelf (see summary in Snedden and Galloway, 2019). Since the 1980s, interest shifted to present-day deep water and below the extensive salt canopy (Figure 5). Cenozoic reservoirs with significant remaining undiscovered resources can be found in the Paleogene and Neogene section with reservoir paleoenvironments ranging from upper slope confined channels to lower slope aprons to abyssal plain submarine fans (Figure 7B–D).

In the Cenozoic are a wide variety of reservoir depositional styles (Figure 7). Important examples include deposits of high-density turbidities, with characteristic trough cross-bedding (tractional trough) indicating tractional flows in the Wilcox play of the Alaminos Canyon, Keathley Canyon, and southern Walker Ridge protraction blocks (Figure 7B). This bedding type and massive Bouma Ta beds form some of the best reservoirs with high porosity (15%–23%), permeability (10–100 md), and low silt (<20%–30%) and clay (<5%) content (Marchand et al., 2015).

Miocene reservoirs show a range of reservoir types from confined channel fills of the paleo upper slope to distributive lower slope systems and abyssal plain fans (Snedden and Galloway, 2019). At the Thunderhorse field in the MC protraction block, thick amalgamated submarine fan deposits are dominated by massive Bouma beds with local scouring and avulsions as indicated by mud clast–rich zones (Figure 7C). Directional information from image logs shows broadly unimodal flows entering the salt-defined Boarshead basin (Henry et al., 2017).

Pliocene–Pleistocene deep-water sandstones deposited in minibasins adjacent to salt diapirs and/or

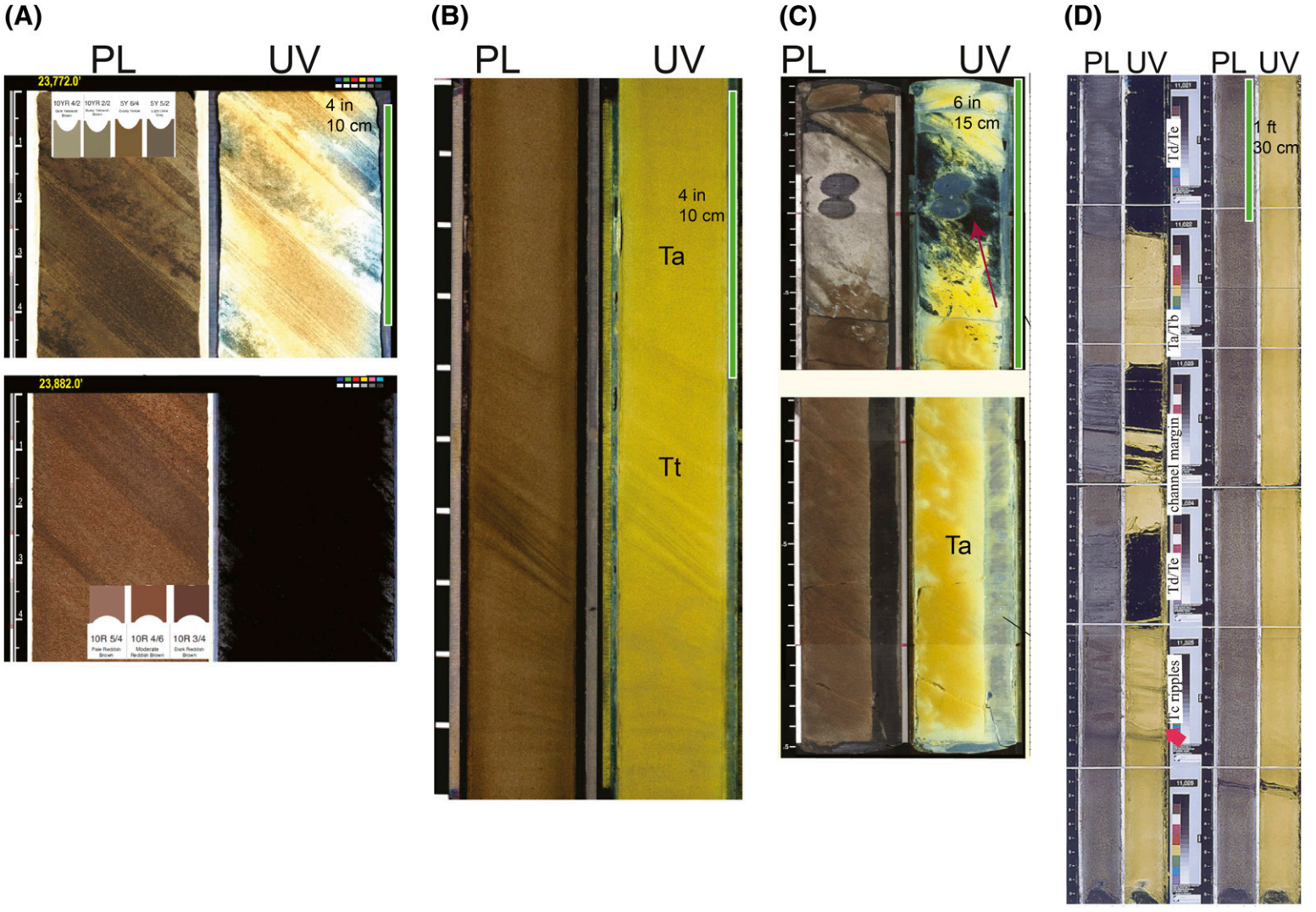

Figure 7. Well cores of important reservoir types in the offshore northern Gulf of Mexico Basin. Both plain light (PL) and ultraviolet (UV) light are shown, with gold to yellow colors indicative of the presence of oil. (A) Jurassic Norphlet aeolian sandstones in Gettysburg well (Desoto Canyon 398-1, see the Appendix) showing high-angle cross-beds formed in aeolian dunes. Lower photograph is below the oil–water contact and thus does not show UV fluorescence. From Godo (2019) and reproduced with permission from the Gulf Coast Association of Geological Societies. (B) Wilcox high-density massive Ta and tractional trough (Tt) bedding formed in confined deep-water flows. From Zarra (2007). (C) Massive Bouma Ta bed and overlying scoured mud-clast zone from the Thunderhorse field Miocene submarine fan reservoir. From Henry et al. (2017). (D) Pleistocene Diana field confined channel-fill sandstone reservoirs showing massive Bouma Ta beds of channel axis and Tc, Td/Te, and Te beds of channel margin, Diana well no. 3 (see the Appendix). Red arrow points to Bouma Tc rippled bed above a basal scour. From Sullivan et al. (2004). For Bouma sequence description, see Bouma (1962).

above the allochthonous salt canopy represented the first phase of northern GOM deep-water exploration. Reservoir styles ranged from highly confined channels with massive Ta beds and scours (Figure 7D; Diana field in Sullivan et al., 2004), Ta-dominated channel terminus submarine fans (e.g., Mars Field in Meckel et al., 2002), and channel–levee systems (e.g., Genesis field in Sweet and Sumpter, 2007).

Reservoir Summary

As mentioned earlier, one criterion for a super basin is the presence of multiple, often stacked or amalgamated reservoirs that facilitate discovery and development and ensure alternative reservoirs in the case of stratigraphic pinch-outs, fault-outs, and erosion. The fields and discoveries of the greater GOM offer a wide diversity of reservoir types ranging from dryland aeolian dune sandstones of the Norphlet to deep-water sediment gravity flow deposits (Figure 7). For further details on the stratigraphic occurrence, areal distribution, and characteristics of these reservoirs, the reader is directed to Snedden and Galloway (2019).

SOURCE ROCKS

Most super basins are the habitat for two or more rich source rock intervals (Sternbach, 2020). Powering the northern GOM Super Basin are three primary marine source rocks centered in the Oxfordian, Tithonian, and Cenomanian–Turonian Stages. Minor deltaic to marine sources have been noted within the Paleocene–Eocene Epochs (Wenger et al., 1994; Hood et al., 2002; Ferworn et al., 2003), as well as other lean marine sources in other intervals, including the Aptian and Albian (Comet, 1992; Figure 8).

The regional extent of petroleum systems charged by these three primary source rocks and Cenozoic terrestrial-dominated shales is displayed in Figure 9. Through geochemical studies of petroleum recovered from reservoirs, surface seeps, and the source rocks themselves, the three primary intervals are proven to have generated large volumes of hydrocarbons both nshore and offshore as conventional and unconventional resources. The Upper Jurassic and mid-Cretaceous sources are synchronous with those in other circum-Atlantic, Arctic, and Tethyan Super Basins because of similar tectonic, eustatic, and climatic drivers following post-Pangaea breakup. Common associations are with restricted rift basins and global OAEs that enhanced and preserved organic matter (Figure 8). In the northern GOM, these primary sources are widespread (Figure 9) but occur in temporally discrete intervals. We summarize Mesozoic source rocks in ascending age order below.

Oxfordian-Centered Source Rocks

Exploration in the onshore salt basins pointed to the Oxfordian Smackover Formation as a source for carbonate-sourced oils in northern GOM (Oehler, 1984; Sassen et al., 1987; Sassen, 1988, 1990; Claypool and Mancini, 1989; Wenger et al., 1994). This source interval was deposited as the GOM transitioned from shallow Louann Salt pan to increasingly deeper-marine conditions. Discoveries in the northern GOM shelf and Norphlet deep-water play of the eastern GOM have also been linked to the Oxfordian source, stratigraphically positioned in the middle Smackover member (Godo, 2019). The distinctive geochemical signature of oils from this source identifies a separate GOM petroleum system (Wenger et al., 1994; Hood et al., 2002; Ferworn et al., 2003).

The quality and stratigraphic variability of the Oxfordian source in the deep-water GOM, the habitat for discovered mean UTRR more than 5 BOE (Bureau of Ocean Energy Management, 2017; Figure 4), is illuminated by detailed geochemical analyses undertaken within the Petersburg well (DC 529-1; location 10 in Figure 9 and the Appendix). The Smackover here has three members or lithologic units, namely, an upper limestone, middle marl, and lower limestone that correspond approximately to three Smackover Formation members of onshore Alabama (Mancini et al., 1992; Godo, 2019). The middle-laminated marl and the upper section of the lower limestone have the highest overall total organic carbon (TOC) content, distributed across a series of thin beds with documented maximums approaching 3%, uncorrected for thermal maturity (Figure 10; Godo, 2019). Gross thickness of this middle Smackover source interval in deep-water wells is in the 800–1000-ft (244–305-m) range. Kerogen is predominately oil-prone marine, type II to IIS, as determined from hydrogen index (HI) values of 300–500 mg HC/g TOC in richer, less mature samples, pseudo-Van Krevelen

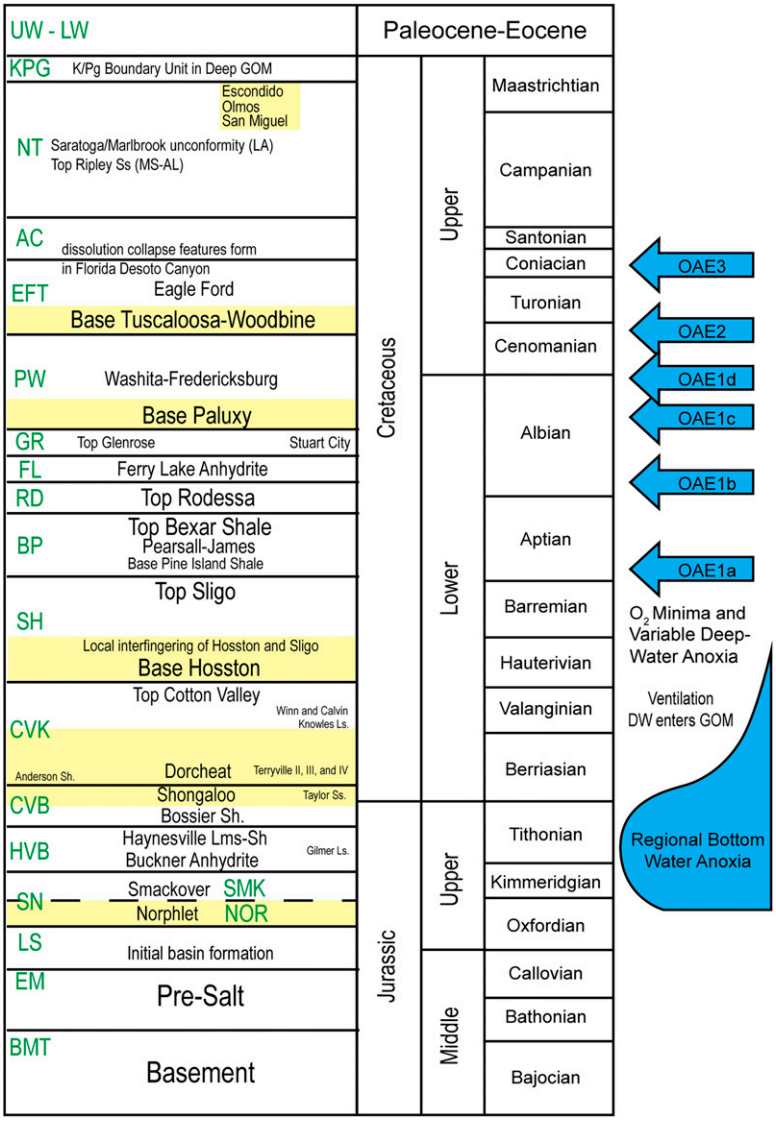

Figure 8. Stratigraphic occurrence of important Mesozoic source rocks of the northern Gulf of Mexico (GOM). Corresponding oceanic anoxic events (OAE) and other paleo-oceanographic events shown to the right of the stratigraphic column. Major sandstone intervals are shown in yellow color along with Gulf of Mexico Basin Depositional Synthesis project chronostratigraphic units shown in green text. AC = Austin Chalk; BMT = basement; BP = Bexar–Pine Island Shale; CVB = Cotton Valley–Bossier; CVK = Cotton Valley–Knowles; DW = deep water; EFT = Eagle Ford–Tuscaloosa; EM = Eagle Mills; FL = Ferry Lake Anhydrite; GR = Glen Rose; HVB = Haynesville–Buckner; KPG = Cretaceous Paleogene; K/Pg = Cretaceous Paleogene boundary unit; LA = Louisiana; Lms-Sh = limestone and shale; LS = Louann Salt; Ls. = Limestone; MS-AL = Mississippi-Alabama; NOR = Norphlet; NT = Navarro–Taylor; PW = Paluxy–Washita; RD = Rodessa; SH = Sligo–Hosston; Sh = shale; SMK = Smackover; SN = Smackover–Norphlet; SP = Sparta; Ss. = sandstone; UW - LW = upper Wilcox–lower Wilcox.

diagrams, and hydrocarbon potential versus TOC plots (Smith, 2018). Well rotary cores in the lower part of the lower limestone member display algal laminites to microbialite growth structures with a lower overall average TOC compared to the middle marl (Godo, 2019). Thermal maturity indicators such as the temperature at which the maximum rate of hydrocarbon generation occurs in a kerogen sample during pyrolysis analysis (T_{max}) and vitrinite reflectance show the Smackover source rocks are in the oil window over much of the deep-water play area leading to generation of light oil (Smith, 2018; Godo, 2019). In shallower waters where deep crustal derived heat flow is considerably higher, reservoired oils have cracked to dry gas with associated H_2S and CO_2 (Mankiewicz et al., 2009).

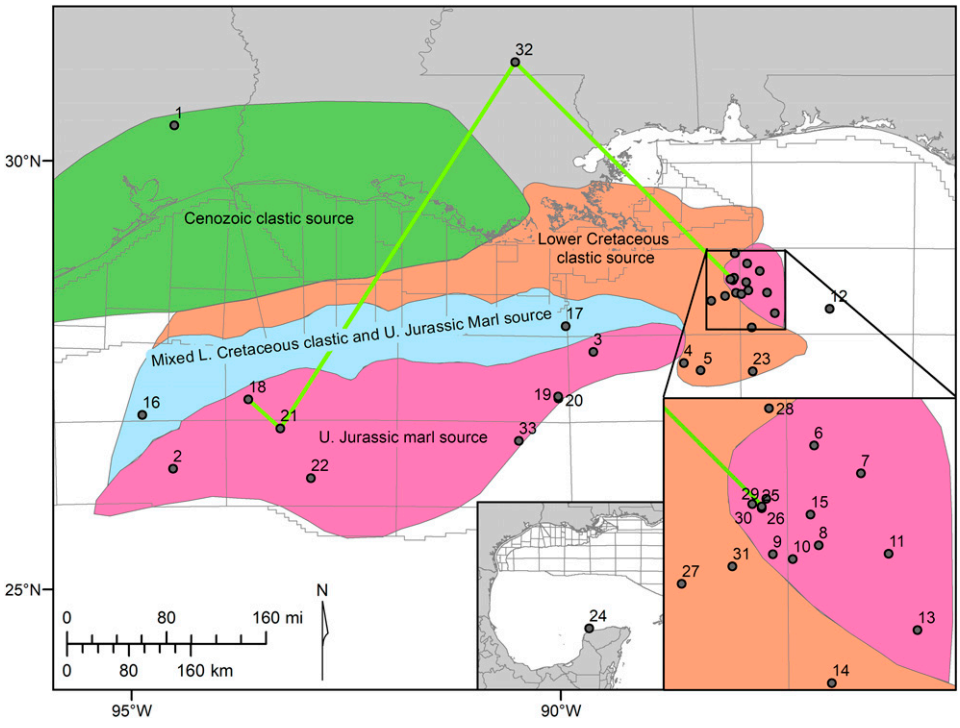

Figure 9. Location of important northern Gulf of Mexico oil families and source rock ages. The primary source rock on the slope is considered to be of Upper (U.) Jurassic (centered on the Tithonian) age and marly carbonate. Mixed families are shown in hachures. Modified from Ferworn et al. (2003), Cunningham et al. (2016), and Weimer et al. (2017a), which is reproduced with permission of *AAPG Bulletin*. L. = Lower.

Upper Oxfordian Smackover source rocks have been linked to seeps and shows over a large area of the basin (Hood et al., 2002; Pepper, 2016) and to the giant oil field on production at Appomattox and numerous other discoveries being considered for development in the MC and DC protraction blocks (Smith, 2018; Godo, 2019).

Tithonian-Centered Source Rocks

Tithonian-centered source rocks, referring to zones of organic enrichment within the Cotton Valley–Bossier (CVB) and Haynesville–Buckner (HVB) supersequences (Figure 11), were recognized early on from seep and reservoired oil analyses in the northern GOM (Figure 9; Comet et al., 1993; Wenger et al., 1994; Cole et al., 1999, 2001; Hood et al., 2002; Ferworn et al., 2003). Biomarker and other geochemical analyses used in these studies demonstrated that the Tithonian-centered petroleum system was generated from clearly different, variably more marly or more siliciclastic-rich source rocks and thus separate from the Oxfordian. Tithonian-centered calcareous to marly source rocks have also been found to have charged fields in the Mexican GOM from the Golden Lane to the Campeche (Gonzáles-Garcia and Holguín-Quiñones, 1992; Yurewicz et al., 1997; Guzman-Vega, 2000; Santamaria Orozco, 2000; Guzmán-Vega et al., 2001; Guzman-Vega and Mello, 2001; Magoon et al., 2001; Holguín-Quiñones et al., 2005; de Lourdes Clara Valdés et al., 2009) and the Varadero heavy oil field in Cuba (Schenk, 2008).

Despite the voluminous geochemical evidence of a Tithonian-centered source in deep offshore areas, there was remarkably little published calibration until quite recently. With the growing body of well-log data in the Mesozoic (Weimer et al., 2016a, 2017b), acquired through drilling of the deep-water Wilcox and Norphlet plays, Cunningham et al. (2016) employed Δ log R, a petrophysical approach using logs calibrated against TOC measurements from sidewall cores and cuttings, to evaluate variation in organic enrichment in Tithonian shales in deep-water areas of the northern GOM. These variations were compared to oil family and source lithofacies interpretations based on reservoired oil and seafloor seeps using an industry proprietary database (GeoMark Research Ltd., 2016, J. Zumberge, personal communication). A key calibration well is the Norton prospect (GB

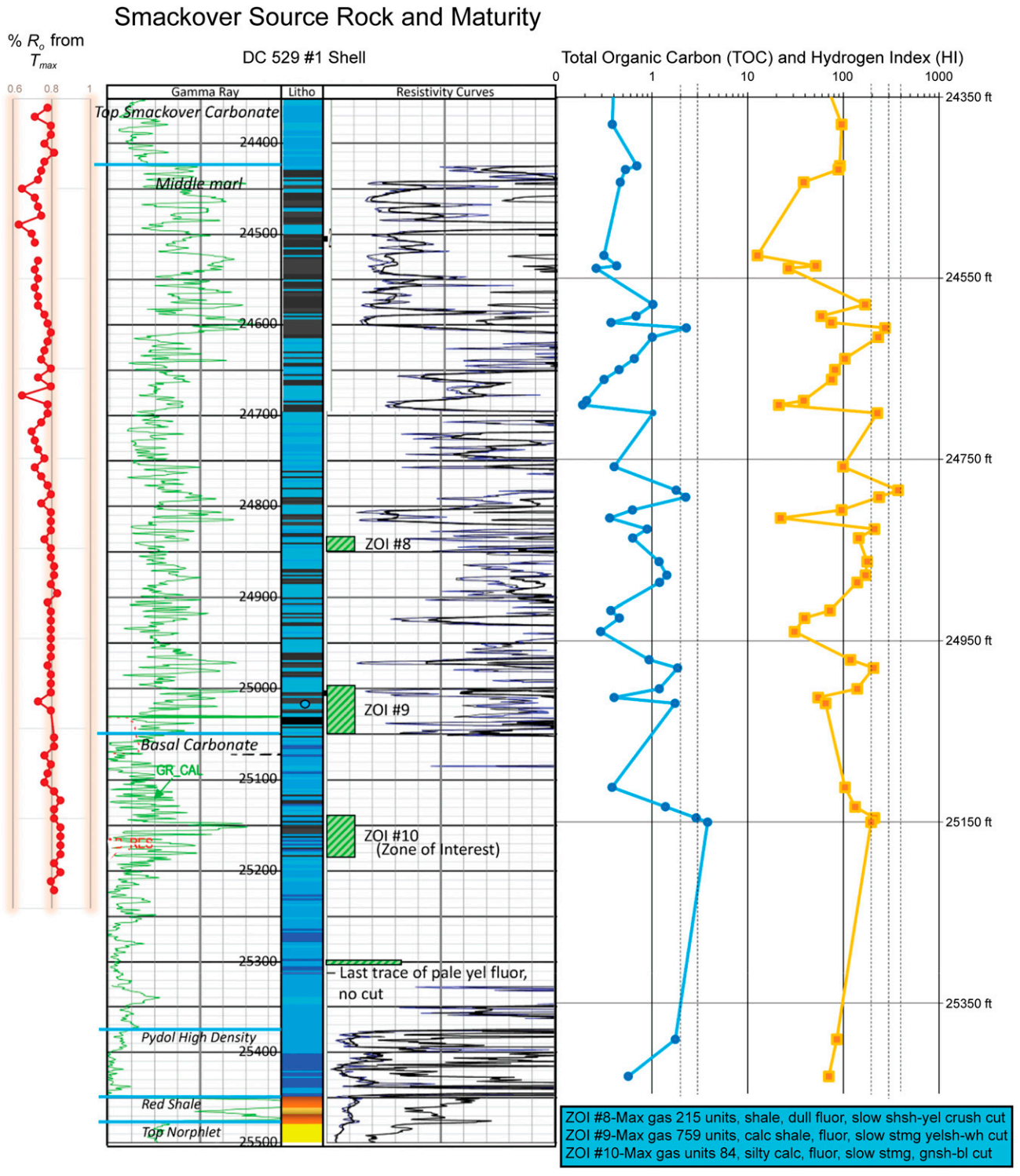

Figure 10. Example of Oxfordian source interval characteristics in the Petersburg well (Desoto Canyon [DC] 529-1, see the Appendix), northern Gulf of Mexico. Modified from Godo (2019) and reproduced with permission from the Gulf Coast Association of Geological Societies. % R_o = % vitrinite reflectance; calc = calcareous; fluor = fluorescence; gnsh-bl = greenish-brown; GR_CAL = caliper; Litho = lithology; Max = maximum; PyDol = pyritic–dolomitic zone; shsh-yel = slight sheen of yellow; stmg = streaming; T_{max} = the temperature at which the maximum rate of hydrocarbon generation occurs in a kerogen sample during pyrolysis analysis; yel = yellow; yelsh-wh = yellowish-white.

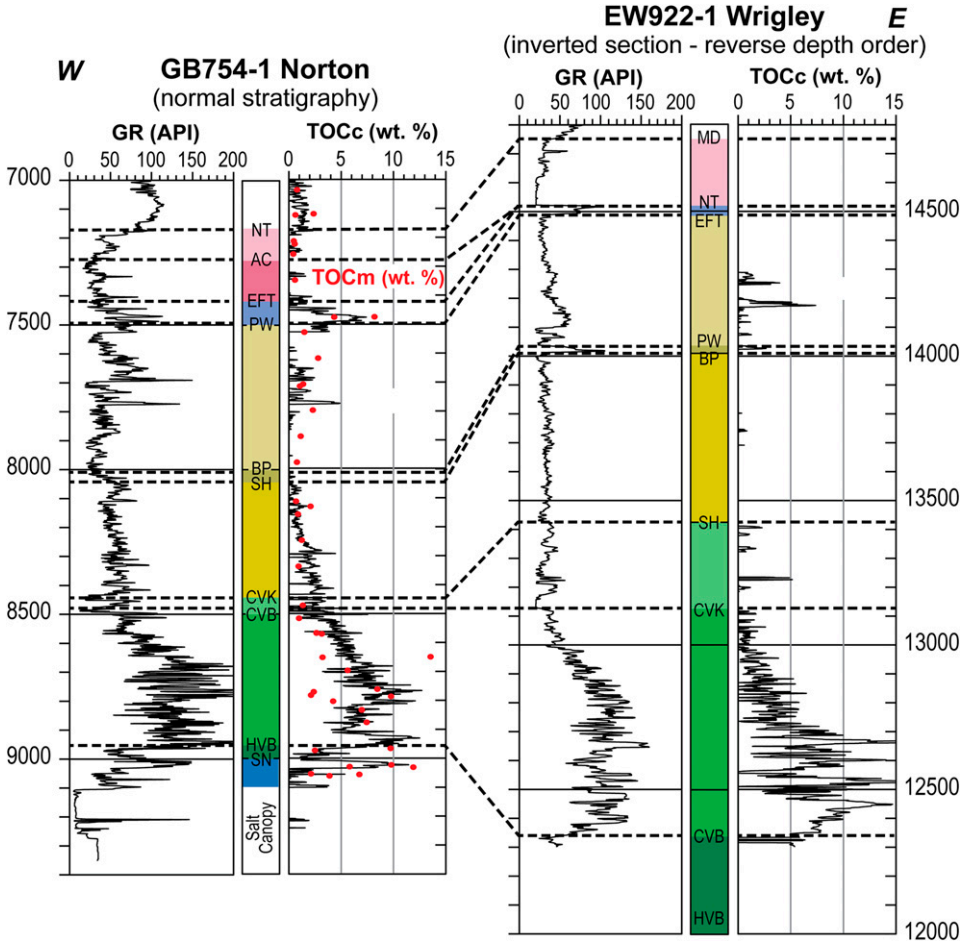

Figure 11. Example of Tithonian-centered source rock intervals in two key wells in the northern Gulf of Mexico. Estimated total organic carbon content from Δ log R calculations. An inverted (salt-overturned) Jurassic–Cretaceous carapace section is shown in the Ewing Bank protraction block (EW) 922-1 well (see the Appendix) in reverse depth order for comparison purposes. Modified from Cunningham et al. (2016). AC = Austin Chalk; BP = Bexar–Pine Island Shale; CVB = Cotton Valley–Bossier; CVK = Cotton Valley–Knowles; EFT = Eagle Ford–Tuscaloosa; GB = Garden Banks protraction block; GR = gamma ray; HVB = Haynesville–Buckner; MD = Midway; NT = Navarro–Taylor; PW = Paluxy–Washita; SH = Sligo–Hosston; SN = Smackover–Norphlet; TOCc = total organic carbon calculated; TOCm wt. % = total organic carbon weight % from core plugs (red filled circles).

754-1; Figure 11, location 18 in Figure 9 and the Appendix). Although Norton and the correlative well Wrigley (Ewing Bank [EW] 922-1; location 17 in Figure 9 and the Appendix) are salt raft or carapace penetrations (for definitions, see glossary in Snedden and Galloway, 2019), biostratigraphy suggests stratigraphic condensation did not occur until later in the salt structure's history and the Upper Jurassic is relatively complete. The Wrigley interval was overturned by salt later in its history (Cunningham et al., 2016). Both wells show the log-derived TOC profile increasing upward from the top HVB surface to the CVB midpoint with values exceeding 10% TOC (log and sample derived) and then declining through the upper CVB and through the overlying Cotton Valley–Knowles interval (Figure 11). They also show net interval thicknesses >300 ft (>91 m) with organic enrichment of more than 5% TOC (log derived), indicating excellent source quality and strong oxygen deficiency in the CVB depositional environment. Other wells extend the observation of organic enrichment more than 5% TOC (log and sample derived) in the CVB across the central GOM to the east (Figures 9, 11).

Given the similar log patterns and levels of organic enrichment at Norton, Wrigley, and other wells (Cunningham et al., 2016), anoxia is suggested to have existed broadly during Tithonian source deposition as the developing GOM ocean basin deepened and became more restricted during drift and thermal cooling. The deep basin remained

starved and density stratified through the Tithonian and into the Berriasian (Cunningham et al., 2016). Furthermore, organic extracts from Upper Jurassic samples of the Norton show high levels of the biomarker bisnorhopane (Jarvie et al., 2004), which is enriched in source rocks deposited under anoxic conditions (Peters et al., 2007). The organic facies of the Tithonian source is type II to IIS marine oil prone, with HI values in richer, less mature samples ranging from 500 to 650 mg HC/g TOC (Jarvie et al., 2004; Peters et al., 2007). Tithonian organic enrichment in the Campeche Sound in Mexico can range even higher above 20% TOC and 700 mg HC/g TOC with the type IIs kerogen rich in sulfur (Santamaria Orozco, 2000). Sulfur content of Tithonian-sourced oils in northern GOM varies spatially, ranging from <0.5% in more clay-rich lithofacies to almost 4% in more carbonate-rich lithofacies, and generally decreases to the west because of the increasing influence of the deep-water Cotton Valley clastic apron (Cunningham et al., 2016). The gross thickness of the Tithonian source averages 700 ft (213 m) in both the northern and southern GOM. Thermal maturity of the Tithonian source grades progressively from dry gas along the outer shelf and upper slope to wet gas and condensate in the midslope to oil over the broad expanse of the lower slope in the northern GOM (Weimer et al., 2016a).

The Tithonian-centered source rocks also extend to onshore areas where the Bossier Shale and Haynesville Shale (or marl) are important unconventional (source rock) plays (Cicero et al., 2010; Hammes et al., 2011). In offshore areas, Tithonian-centered sources are particularly important in the northern United States GOM and over the giant field province of the Akal–La Reforma trend in Mexico (Guzman-Vega and Mello, 1999; de Lourdes Clara Valdés et al., 2009). Based on the spatial agreement with the Tithonian-centered oil family composed of reservoired oils and seeps, a large part of the 22 BOE UTRRs estimated for the Wilcox subsalt play in the deep-water GOM (Figures 4, 9) is thought to be derived from the Tithonian-centered source rock.

Cenomanian–Turonian-Centered Source Rocks

Cenomanian–Turonian Eagle Ford–Tuscaloosa (EFT) supersequence mudstones and other Cretaceous shales are well-documented hydrocarbon source rocks for onshore unconventional plays (Hentz and Ruppel, 2011; Hull et al., 2012; Hammes et al., 2016; Zumberge et al., 2016) and for the charge of conventional plays in the offshore (Hood et al., 2002; Ferworn et al., 2003). Many of the zones of enriched and preserved organic matter in this time span are linked to oceanographic conditions associated with major carbon isotope–constrained OAEs (Figure 8). The OAEs are geologically brief (<1 m.y.) episodes of oxygen-depleted conditions in the global ocean that resulted from profound perturbations in the carbon cycle. They were originally defined as intervals of globally synchronous black shale deposition (Schlanger and Jenykns, 1976), but subsequent work has shown that individual black shales are often diachronous (e.g., Tsikos et al., 2004a, b; Lowery et al., 2017), and OAEs are best defined by their positive carbon isotope excursion (Jenkyns, 2010). The OAEs are driven by a net increase in nutrients in the global ocean and reduced circulation, although the speculation on the causes ranges from continental weathering, volcanism, global warming trends, to globally high sea-level conditions. Early work suggested that source rocks deposited globally during Cretaceous OAEs and in Jurassic anoxic basins could be responsible for up to 50% of the global hydrocarbon endowment (Klemme and Ulmishek, 1991).

In the offshore northern GOM Basin, source enrichment in the Cretaceous is most clearly associated with OAE2 at the Cenomanian–Turonian boundary (Lowery et al., 2017; Figure 8), although pulses of organic enrichment also occur during Aptian–Albian OAEs. The GOM stratigraphic record does not align particularly well with the documented global sea-level highstand and organic enrichment of OAE2 at the Cenomanian–Turonian boundary. The highest organic content within the onshore unconventional Eagle Ford and Tuscaloosa marine shale plays occurs somewhat earlier and later than the OAE2 isotopic excursion, respectively (Phelps et al., 2015; Lowery et al., 2017). It is believed that the timing of anoxia, productivity, and organic enrichment varies locally because of interaction of the basin with circulation outflow events from the adjacent Western Interior seaway and sea-level rise and intensification of the oxygen minimum zone (Lowery et al., 2017).

Organic enrichment within the offshore Cenomanian–Turonian section can be quite high, with

documented TOC values ranging more than 7% at Norton (GB 754-1; Figure 12) and more than 4% at Cheyenne (Lloyd 399-1; location 23 in Figure 9 and the Appendix). Type II marine kerogen is indicated by HI values ranging from 400 to almost 600 mg HC/g TOC at both wells. The thickness of the richest interval in the EFT, presumably spanning the Cenomanian–Turonian boundary, is approximately 100 ft (~31 m). However, dilution of the source by voluminous siliciclastic influx by the Tuscaloosa deep-water system (Snedden et al., 2016; Lowery et al., 2017) can reduce TOC in the submarine fan axes in the central GOM. The Cenomanian–Turonian source is thought to be most important in charging or contributing to charge in the Wilcox reservoirs of the northern Alaminos Canyon, EW, GB, and GC protraction blocks, and shelfal areas, where oil quality may be improved by mixing with higher-sulfur Tithonian-sourced oils (Figure 9; Eikrem et al., 2010).

Other Lower Cretaceous source rocks are known in the onshore and offshore northern GOM and are typically associated with other marly to shaley OAE intervals. They occur within the Albian Mesilla Valley Shale and Boracho Formations on the Comanche shelf in Texas in association with OAE 1d and c, respectively (Scott et al., 2020; Figure 8), the Albian Glen Rose and Sunniland Formations in Texas and Florida, respectively, in association with OAE 1b (Palacas et al., 1984; Sun and Forkner, 2019), the Aptian–Albian Bexar Shale and Pine Island Shale Members of the Pearsall Formation in South Texas in association with OAE 1b and a (Hackley et al., 2009; Hull, 2011; Hackley, 2012b; Hull et al., 2012), and within several Albian-Berriasian intervals observed in Deep Sea Drilling Project boreholes in the Straits of Florida (Katz, 1984; Cole et al., 1999). However, although these occurrences may be rich, they are believed to be more geographically restricted (Enomoto et al., 2012; Hackley, 2012b; Swanson et al., 2013a; Merrill, 2016).

Critical Moment of Source Rock Maturation and Migration

Source richness, distribution, and maturity are just some of the necessary components of an economically valuable petroleum system. An equally relevant process in all super basins is how the critical moment of generation and migration of hydrocarbons relates to the earlier phases of reservoir–seal pair deposition and trap development (Sternbach, 2020). The role of the allochthonous salt canopy in delaying source rock maturation in the deep-water GOM is an underappreciated yet critical factor in allowing this basin to be the habitat of such a large hydrocarbon endowment (Ewing, 2016; Figure 13). Oil and gas maturation windows are relatively shallow in onshore basins where continental crust heat flow is high and widely separated diapirs only locally influence maturation processes. Thus, at present, most of the lower Mesozoic source rocks are generating gas in areas like East Texas. This pattern continues to the shallow-water offshore areas where both heat flow decreases marginally but the absence of salt caused by loading and evacuation is still a concern. However, in the area of the allochthonous salt canopy, the nearly continuous salt body transfers heat away from the subsalt areas, effectively deepening the oil and gas windows (Figure 13). This process is accompanied here by reduced heat flow on transitional and oceanic crust, cooler seabed temperatures, and later burial by Cenozoic strata (Husson et al., 2008). The net result is a delay in maturation and primary migration so that Mesozoic source rocks remained viable hydrocarbon generators longer than without a salt canopy (Ewing and Galloway, 2019). Salt tectonics in the deep-water areas continued to nearly present day (Hudec et al., 2013) enhancing cross-stratal vertical migration (Hood et al., 2002) and later trap development and filling, which has significantly increased the overall number of economically attractive hydrocarbon accumulations.

Seal Rocks

Effective seal rocks are also a critical component of petroleum-rich super basins. Seal rocks, which in the GOM Basin vary from shales to carbonate mudstones to evaporites, trap and retain large columns of oil and gas. Competent seals limit significant loss of hydrocarbons caused by capillary leakage, maintaining large hydrocarbon columns over geologic time frames, as evidenced in many large accumulations in the northern GOM migrating from source rocks as old as the Oxfordian (Jurassic) as described in the preceding section.

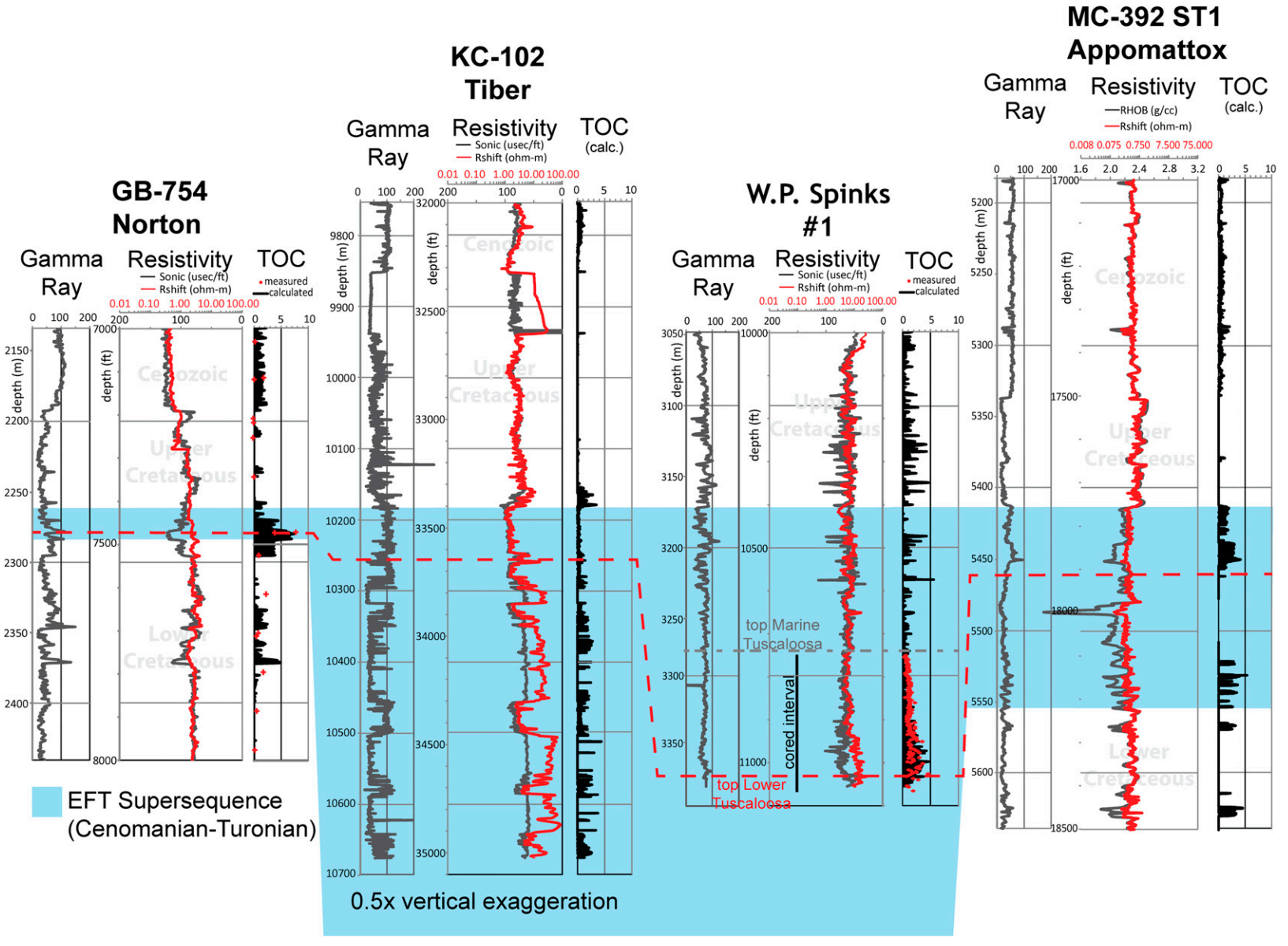

Figure 12. Example of Cenomanian–Turonian source rock interval in four key wells in the northern Gulf of Mexico. Estimated total organic carbon (TOC) content from Δ log R calculations. Modified from Lowery et al. (2017). calc. = calculated; EFT = Eagle Ford–Tuscaloosa; GB-754 = Garden Banks protraction block 754; KC-102 = Keathley Canyon block well-102; MC-392 ST1 = Mississippi Canyon block 392-1 sidetrack-1; RHOB = density log; Rshift = resistivity shallow induction.

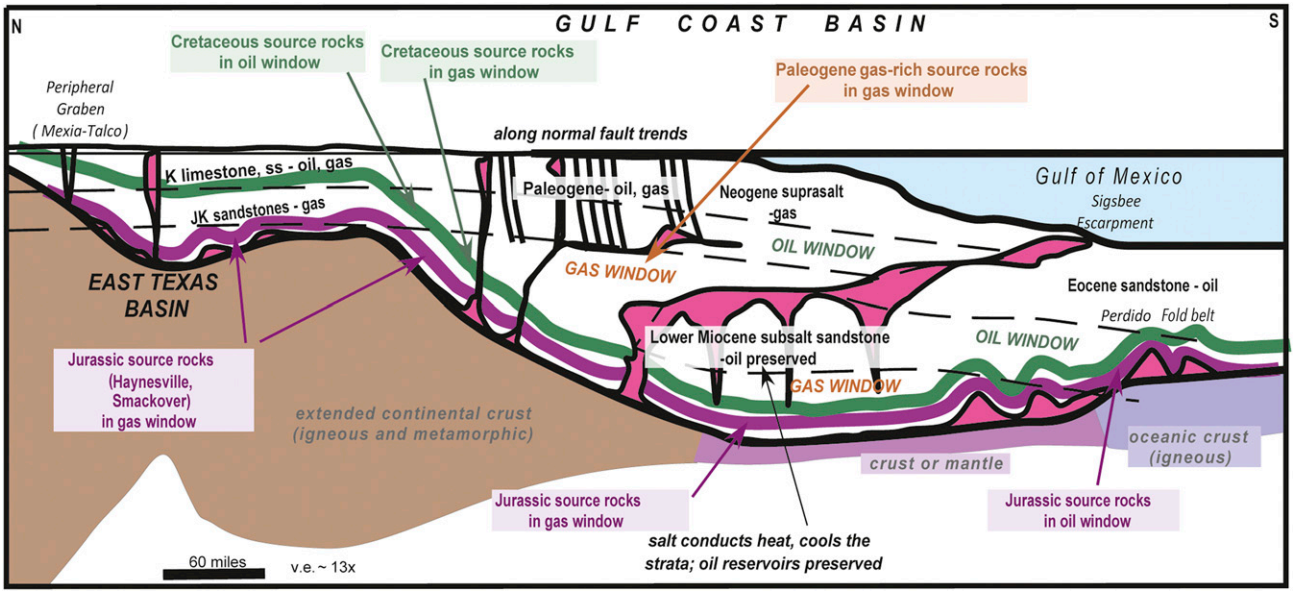

Figure 13. Generalized petroleum system framework of the northern Gulf of Mexico margin. The section generally extends from the East Texas basin southward across the coastal plain, continental shelf, slope, and onto the abyssal plain. From Ewing (2016) with permission from the Bureau of Economic Geology. JK = Jurassic–Cretaceous; K = Cretaceous; ss = sandstone; v.e. = vertical exaggeration.

For the purpose of this discussion, we focus on the geologic factors inherent to the GOM that limit capillary leakage through the top seal. We specifically exclude fault-dependent traps in which sealing along faults results from development of fault gouge, continuous shale smears, and zones of cataclasis (deformation bands), which are controlled by local deformation and other prospect-specific factors.

Mechanical failure of seal rocks is known to occur in situations in which fluid pressures within the reservoir exceed a critical threshold (fracture or lithostatic gradient), causing a major loss of mobile hydrocarbons and leaving a smaller amount of live (moveable) oil or just residual oil. Although this does occur in the GOM Basin, it is not a pervasive risk element, as evidenced by the large GOM hydrocarbon endowment. In addition, in exploration of northern GOM minibasins above salt, where steep dips and rapid burial occur, subsurface pressures can exceed the minimum principal stress and leakage occurs to the surface until pressures fall below the threshold preserving commercial hydrocarbon columns in the case of Popeye and Genesis fields in GC (Seldon and Flemings, 2005).

Despite the abundant discovered resources in the basin, relatively few published studies have specifically analyzed the capillary seal rocks that trap hydrocarbons here. Seal rock integrity can be evaluated in several ways. First, experimental work on cuttings and core samples is conducted to establish the distribution of pore-throat sizes, often with a nonwetting fluid such as mercury. Second, preproduction pressure data (e.g., modular formation dynamics tester™ [MDT; Schlumberger] or reservoir characterization instrument™ [RCI; Baker Hughes]) from the field or discovery provide an indication of the seal competency because offsets in fluid pressure mark an effective barrier to fluid pressure communication over geologic timescales. We discuss the evidence from both approaches in the GOM below.

Experimental Analyses on Northern Gulf of Mexico Basin Seals

Capillary or membrane seals trap hydrocarbons in structural closures or along bounding faults (Downey, 1984). Column height is controlled by the pore system of the sealing lithology because the largest pore throat serves as the weak point allowing leakage until buoyancy forces equalize the opposing capillary forces (Jennings, 1987). Other influencing factors are the interfacial tension between various fluids, oil, water, gas, and CO_2 (Schowalter, 1979). Pore systems in shales and carbonate mudstones are measured using mercury (Hg) injection at high pressure (MICP), yielding important parameters such as the

approximate entry pressure and pore-size distribution, with corrections for closure and conversion to hydrocarbon–water systems and adjustments for hydrocarbon composition, temperature, and pressure (Wardlaw and Taylor, 1976).

Using a combination of MICP, compositional, and petrophysical analyses over several GOM Miocene deep-water shales, Dawson and Almon (2005) identified six end-member seal types (Table 1). The six identified type shales (mudstones and claystones) range from seal type 5 silty laminated shale (including microporous quartz) with the lowest entry pressure (MICP at 10% Hg saturation) to seal type 1 carbonaceous shales with low silt content and highest entry pressures.

Dawson and Almon (2005) also estimated expected hydrocarbon column heights for the Miocene deep-water seals using parameters conditions known to exist at the depth from which each sample was collected, including subsurface temperatures, water and hydrocarbon density, and grain size (Table 1). Corresponding median (50% probability, P_{50}) column heights ranged from 1265 ft (386 m) for seal type 1 to 160 ft (18 m) for seal type 5. All samples were derived from depths greater than 10,000 ft (>3049 m). Compaction was thus well advanced, and differences are thought to be caused by changes in mudstone composition, silt content, and fabric (Dawson and Almon, 2005)

Dawson and Almon (2005) also related seal characteristics to the sequence stratigraphic position of the shale, with the best sealing mudstones, particularly those with high organic content, developed in the upper parts of transgressive systems tracts. Highstand systems tract shales were among the poorest seal rocks, especially where higher silt contacts induced compactional shielding of pores during burial, yielding lower entry pressures and estimated smaller column heights (Table 1). Hentz and Hongliu (2003) also observed that third-order transgressive shales were among the most important hydrocarbon seals in the middle to lower Miocene of shallow waters in offshore Louisiana.

As mentioned in the previous section on source rocks, organic-rich mudstones occur in several Mesozoic transgressive intervals, including the Oxfordian (middle Smackover marl), Tithonian

Table 1. Gulf of Mexico Miocene Deep-Water Shale Seal Types and Predicted Oil Columns

Shale (Seal) Types	Lithology	Clay, %	Carbonate, %	Quartz, %	Total Silt, %	Gamma Ray (°API)	Perm, md	Porosity, %	Bulk Density, g/cc	Capillary Pressure (at 10% Saturation, psi)	P_{50} Oil Column, ft
1	Slightly silty and pyritic, fissile, carbonaceous shale	76	3	12	21	88	0.0006	14.2	2.285	8394	1265
2	Moderately silty, pyritic, and fossiliferous shale	69	5	17	26	127	0.0004	10.3	2.462	7448	1110
3	Moderately silty, fossiliferous, mottled shale	61	4	29	35	122	0.0012	11.9	2.359	4511	855
4	Very silty, pervasively bioturbated shale with mottles	57	4	31	39	88	0.0017	12.4	2.259	3177	375
5	Very silty, carbonaceous shale with microporous siltstone laminae	49	3	37	48	90	0.0058	14.2	2.306	1360	160
6	Slightly silty, pyritic, and fossiliferous, calcareous claystone	64	15	17	21	53	0.0008	13.9	2.283	7653	880

From Dawson and Almon (2005) with permission from the Gulf Coast Association of Geological Societies. Abbreviations: P_{50} = 50% probability; Perm = permeability.

(Haynesville–Bossier shales), Cenomanian–Turonian (Eagle Ford), and other zones. Preservation of organics deposited in these transgressive anoxic events is favored under low-oxygen conditions. This in turn reduces disruption of laminated fabrics by burrowing organisms and thus increases seal capacity (Dawson and Almon, 2005).

Mudstones with enhanced organic content are important in the Cenozoic section, although global anoxic events were not as frequent. Some organic enrichment occurs around the Paleocene–Eocene thermal maximum, as noted in locally restricted basins, because of salinity stratification or paleo-bathymetrical enclosures (Blanke et al., 2009; Cunningham et al., in press).

Mesozoic top seals include carbonate mudstones such as in the case of the Jurassic Norphlet deep-water play. Because the basal Smackover Formation is situated stratigraphically between the middle Smackover marl source and Norphlet sandstones, downward charging migration routes are required and demonstrated for this area (Godo, 2017). Other documented Mesozoic seals occur in the Tuscaloosa Formation, where middle marine shale units above the thick basal sandstone reservoir provide sufficient sealing capacity to hold hydrocarbons or act as barriers preventing vertical migration from CO_2 storage sites (Lu et al., 2011). The MICP measurements of the middle Tuscaloosa mudstone at the Cranfield site indicate that large columns of CO_2 could be retained below the shale during injection, a testament to the good seal integrity.

One caveat about using MICP data as a measure of seal rock capacity is the necessary requirement that a sufficiently large database of MICP be obtained to fully characterize the seals because a small sample set may miss the weakest mudrock that allows vertical leakage. Dawson and Almon (2005) based their classifications upon a large database, although the specific samples or size of the data set were not reported. A second approach, described below, uses the measured downhole fluid pressures to assess the seal capacity, independent of experimental analyses upon the bounding shale beds.

Column heights in subsurface traps have been directly related to the seal capacity of shales through testing and development of empirical relationships such as done by Sneider et al. (1997). However, column height can be controlled by a variety of other independent factors, including ineffective source rocks, fault juxtaposition leakage, overly long charge residence time, or unmapped spillpoints (Aplin and Larter, 2005). The important role of overpressured seal rocks (relative to underlying reservoirs) is also noted in some cases. The timing of overpressuring, however, controls its effect on both reservoirs and seals, and that factor tends to be block or prospect specific.

Subsurface Fluid Pressures as Indicators of Seal Rock Quality

The GOM mudstones with significant lateral or vertical seal capacity are commonly recognized as offsets in downhole pressure measurements (Downey, 1984). The magnitude of offsets may appear to be relatively small when pressure information from downhole measurements is simply plotted versus depth. Smaller offsets can be discerned using the excess pressure technique of Brown (2003). With this technique (described below), subtle yet important pressure changes can be illuminated, especially when recent vintage MDT or RCI data are available. Such an approach is most appropriate when recent vintage MDT or RCI data have accuracy and precision in the 0.01–0.002-psi (0.07–0.01-kPa) range versus older strain gauge data with accuracy of 1.01% (Chen, 2014).

Publicly available downhole pressure data, mainly from modular downhole tools such as the MDT and RCI for deep-water wells, can be obtained from the Bureau of Ocean Energy Management or Bureau of Safety and Environmental Enforcement to illuminate the quality of important seal rocks in Mesozoic and Cenozoic fields and discoveries. All data are first evaluated to eliminate low-quality pressure measurements caused by tool failure or low-permeability rock for which test time length is not sufficiently long enough to achieve equilibrium.

Excess pressure is calculated for reservoirs by selecting nominal fluid gradients that are based on compositional data (if available) or modified iteratively until a vertical line in the same fluid phase is achieved (assuming limited gravity segregation). The methodology is described in detail by Brown (2003).

We consider the seal rocks from two of the most important reservoirs in the basin, the Paleogene Wilcox and Jurassic Norphlet. These represent the largest

and newest deep-water resources by UTRR, respectively (Figure 4).

Jurassic (Oxfordian) Seal Rocks

As mentioned, the Norphlet Formation is the newest and second most important reservoir (by UTRR) in the deep-water GOM (Figure 4). Whereas hydrocarbon production from the Norphlet dates back at least 30 yr, the deep-water play opened in 2011 with the drilling of the Shiloh prospect in the DC protraction block (Godo, 2017; location 7 in Figure 9 and the Appendix). Subsequent drilling of a variety of trap types ultimately led to discovery of the giant Appomattox field in 2010 that began production in 2019. The main top seal to the Norphlet is a carbonate limestone, the basal member of the Smackover Formation (Godo, 2019). Analysis of publicly available downhole pressure data allows one to estimate its ultimate seal capacity; it is also an opportunity to consider other factors that control the size of hydrocarbon accumulations in this complex play. We consider below the basal Smackover seal in the largest Norphlet deep-water discovery to date, the Appomattox.

The Appomattox discovery well (MC 392-1 sidetrack 0 bypass 0; Figure 14, location 25 in Figure 9 and the Appendix) encountered a large oil column with penetrated oil down to the base of Norphlet reservoir (Godo, 2019). Several sidetracks from the vertical well were drilled and sidetrack 2 bypass 1 (ST2BP1) penetrated the oil–water contact (OWC) at 26,265 ft true vertical depth (8007 m) or 26,190 ft true vertical depth subsea (TVDss) (7985 m). Trap crest is estimated to be approximately 24,300 ft (~7409 m), indicating an oil column of 1890 ft (576 m) (Godo, 2019). The shallowest pressure point with good mobility on the well MDT is approximately 24,730 TVDss (~7540 m).

Interpretation of released MDT pressure data from subsequent Appomattox drill wells suggests the presence of at least three separate preproduction (geologic timescale) reservoir compartments: (1) Appomattox South, (2) Appomattox Northeast, and (3) Appomattox Northwest (Figure 14). The largest compartment with the tallest oil column is Appomattox South, delineated by the Appomattox discovery and two sidetracks. The Appomattox MC 391-1 well, when excess pressure is calculated by removing the oil gradient, plots on the same vertical line, indicating that it is part of the same oil compartment (Figure 15).

Appomattox Northeast (MC 348 and MC 392) is a reservoir compartment with a smaller oil column and lower pressure oil (Figure 15). It likely has the same water pressure gradient as Appomattox South because mapping suggests that the aquifer extends around the mapped fault tip-out point to the south (Godo, 2019; Figure 14). Appomattox Northwest is interpreted to have a much smaller column than the other compartments, although this was unproven at the end of appraisal drilling. Preproduction well data (MC 391-1 sidetrack1) clearly indicate that it has a different water pressure than Appomattox South. Compartment boundaries are formed by faults and/or zones of cataclasis (deformation bands) and aeolian reservoir limits (Godo, 2019).

To evaluate the highest penetrated seal capacity for this Norphlet deep-water play, we calculated the oil entry pressure (OEP) for the Appomattox South compartment, the largest yet discovered in the Norphlet deep-water play area. The OEP is determined from the excess pressure plot by measuring the difference between the water pressure and oil pressure at the top of the oil column. The OEP is thus a measure of buoyancy forces that are presently being exerted against the basal Smackover member top seal that traps the penetrated oil column. This is a method of assessing the seal quality independent of the sampling bias issue associated with MICP as described in the preceding section.

The OEP for the Appomattox South compartment was calculated using the Appomattox South oil gradient and the Appomattox Northeast water gradient. For operational reasons, no MDT pressure measurements were taken in the highly deviated MC 392-1 ST2BP1 well that penetrated the OWC in Appomattox South. Using the aforementioned structural crest at 24,300 ft (7409 m), the estimated OEP is approximately 235 psi. Using the highest point of good pressure readings, a minimum value is 180 psi.

These OEP estimates are much larger than that of the adjacent Rydberg well, which we calculated as 87 psi, but this is a minimum value since the trap is known to be underfilled because of a limited source rock fetch area (Godo, 2019). The OEP at Appomattox South is at least 2 to 2.7 times larger,

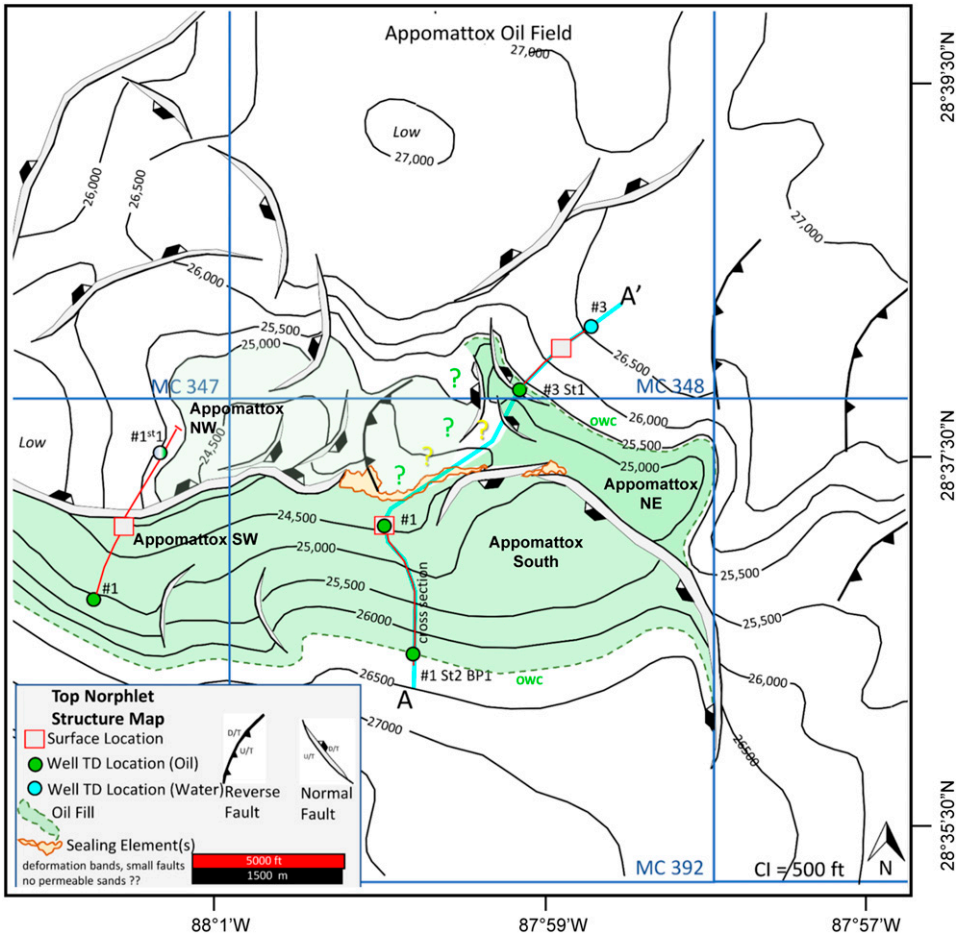

Figure 14. Structure contour map on top of Norphlet Sandstone, Appomattox field area. Contour interval (CI) equals 500 ft (152 m). Modified from Godo (2019) and reproduced with permission from the Gulf Coast Association of Geological Societies. BP = bypass; D/T = downthrown; MC = Mississippi Canyon protraction block; OWC = oil–water contact; St = sidetrack; TD = total depth; U/T = upthrown.

suggesting that this is more representative of the ultimate top seal capacity in this high-pressure, high-temperature play.

This confirms the exceptional seal strength of top seal to the Norphlet deep-water play, one of the most important additions to the United States reserves in the last 10 yr. The presence of an overlying organically enriched, laminated carbonate mudstone of the basal Smackover member, analogous to the Dawson and Almon (2005) seal type 1, is consistent with this.

Another likely enhancing factor is the pressure inversion observed at Appomattox. During drilling at Appomattox and other Norphlet wells, mud weights are usually reduced by at least 1 ppg (from ~14.5 to 13.5 ppg) when entering the Norphlet reservoir (T. Godo, 2020, personal communication) to avoid an abnormally high flow of drilling fluid into the porous formation. This roughly equates to a change in subsurface pressures from 18,850 to 17,550 psi (1.3E5 to 1.2E5 kPa) for a near-balanced well. That pressure inversion probably complements seal rock strength and capacity to trap large oil columns, such as observed in the southern compartment at Appomattox.

Paleogene Wilcox Seals, Cascade Field (Walker Ridge)

The Cascade field, discovered in 2002 by Petrobras, is a four-way closure formed by a contractional fold in the Keathley Canyon–Walker Ridge fold belt (Weimer et al., 2016b). Production began in 2012 and marked the first approved United States GOM usage of a floating production system (Haddad et al., 2012). Reservoirs are present in the Paleogene Wilcox Group, in a water depth of 8200 ft (2500 m). Reservoir porosity is approximately 20% and permeability ranges

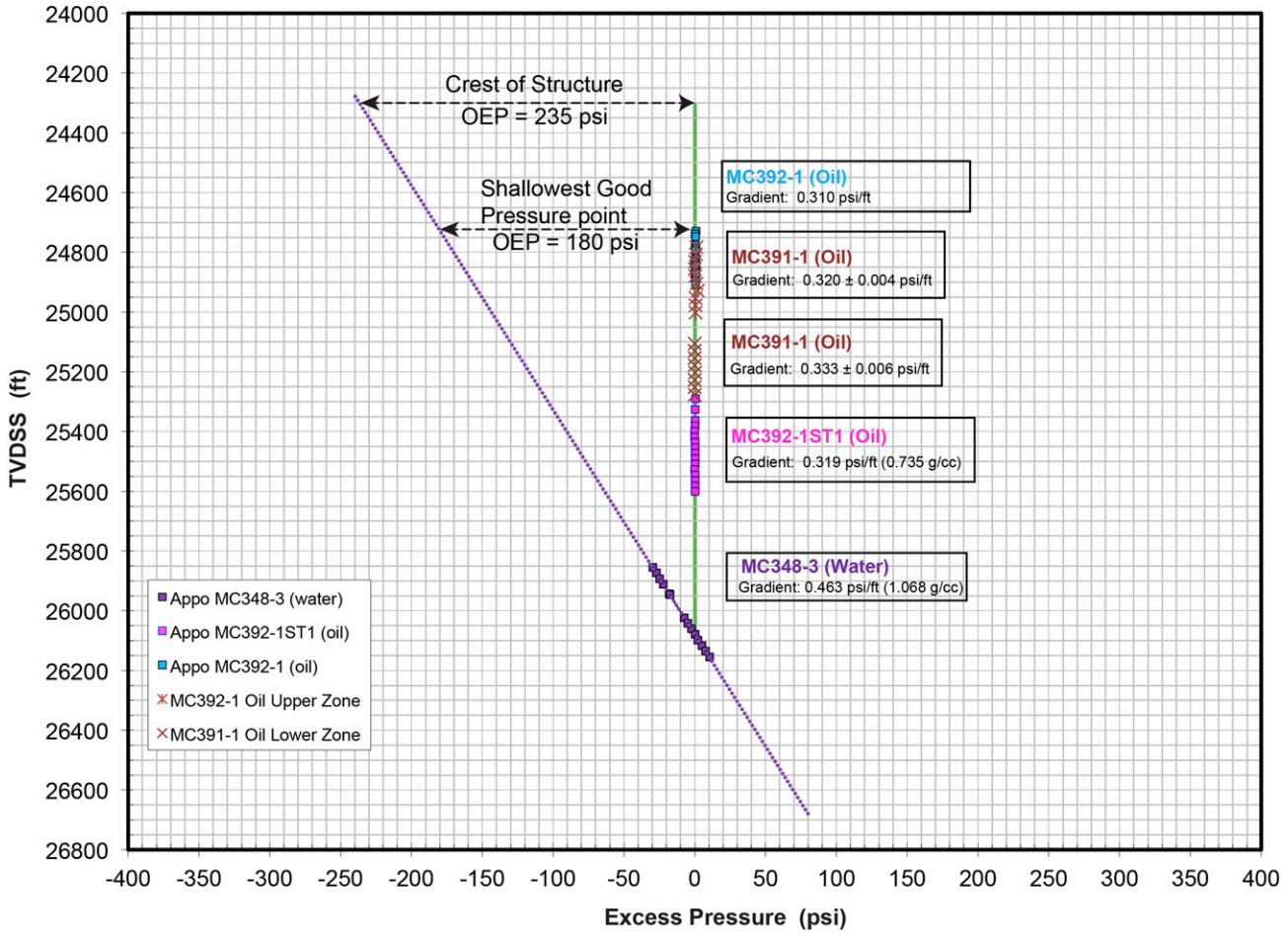

Figure 15. Excess pressure versus depth plot, Appomattox (Appo) South compartment. Water pressures from Mississippi Canyon (MC) 348-3 well (see the Appendix) used for water gradient. Pressure data from Bureau of Ocean Energy Management. OEP = oil entry pressure; ST1 = sidetrack 1; TVDSS = true vertical depth subsea.

from 5 to 50 md with subsea depths of 25,000 ft (7622 m) (Mattos et al., 2013).

The top–sealing lithology is a combination of shale and carbonate mudstone (Figure 16, arrow 1). The Eocene Queen City Formation equivalent and carbonate mudstones of the overlying Sparta Sand equivalent section represent basin-wide condensed intervals (Galloway et al., 2011). This 90–100-ft (27–31-m) section traps a gross oil column of nearly 2000 ft (610 m). The presence of a lithology able to hold such a large oil column is incontestable evidence of excellent sealing capacity, even without MICP testing or calculation of the OEP.

With subsurface pressures of nearly 20,000 psi (1.37×10^5 kPa), important offsets indicating high-quality internal seals and barriers may also be overlooked on normal pressure versus depth (P-D) plots. Use of the excess pressure method (Brown, 2003) and an oil gradient of 0.357 psi/ft (8.08 kPa/m) reveals three prominent pressure offsets across logged shale zones within the Wilcox gross reservoir section in the Cascade WR 250-CA004 well (Figure 16, arrows 2, 3, and 4, well location 33 in Figure 9 and the Appendix). The top of the Wilcox 2 zone is a field-wide shale barrier that is quite subtle on P-D plots but with an offset of 100 psi is better illuminated on the excess pressure plot. This shale is interpreted as a third-order shutdown of Wilcox sand into the Cascade field area (Syrio et al., 2013).

The two lower offsets (labeled 3 and 4 in Figure 16) have larger individual excess pressure differentials exceeding 250 psi (1724 kPa) but are located below the Cascade field oil transition zone. The low overall permeability and common interbedding of shales and silt-rich non–hydrocarbon-bearing sandstones make establishing a single water gradient quite difficult

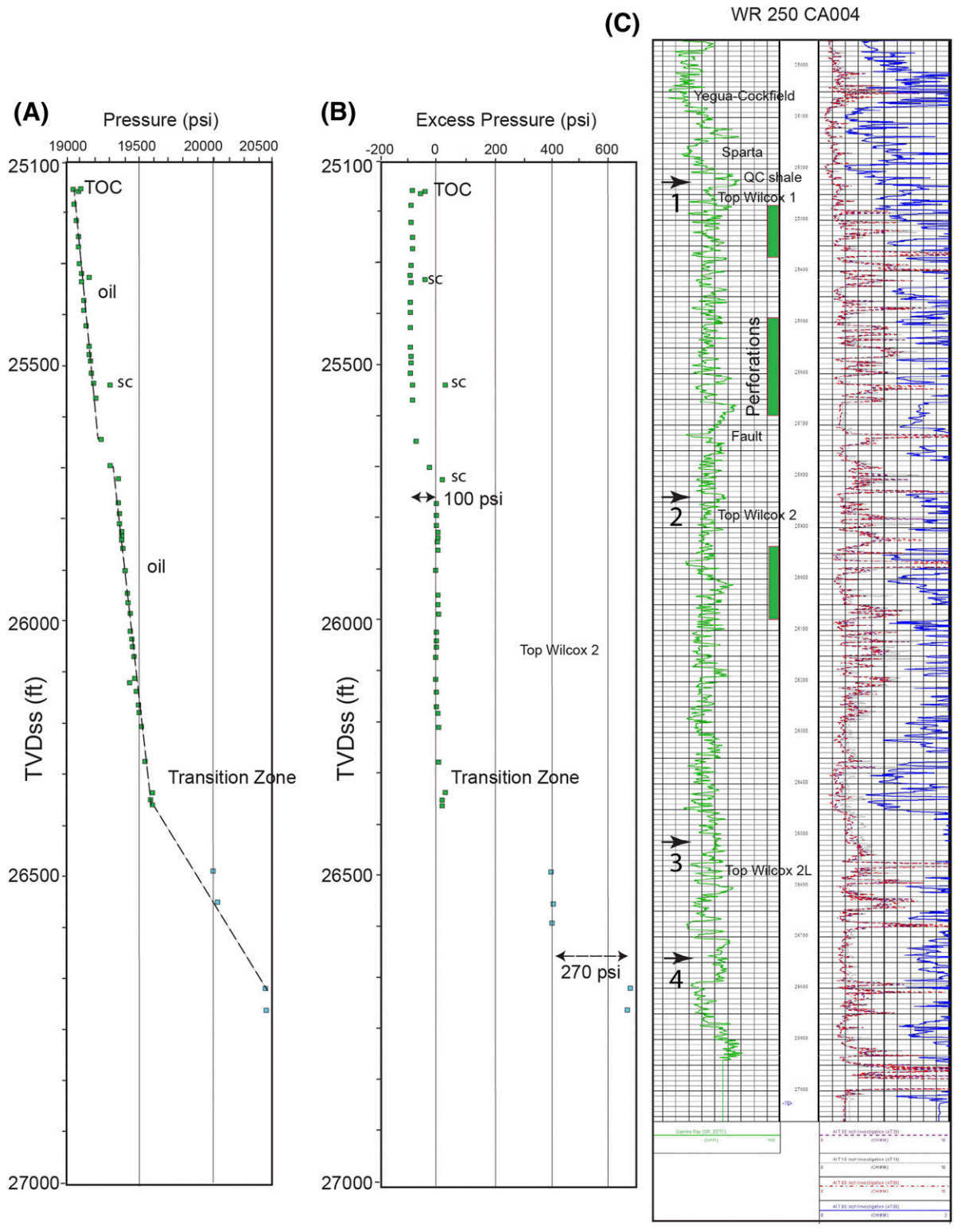

Figure 16. Cascade Walker Ridge (WR) 250 CA004 well. (A) Modular formation dynamics tester pressure versus depth plot. (B) Excess pressure versus depth plot. Oil gradient used is 0.357 psi/ft. (C) Well logs with annotated tops and location of perforations. Pressure data and logs from Bureau of Ocean Energy Management. Field tops from Syrio et al. (2013). Well location in the Appendix. GR_EDTC = edited curve; QC shale = Queen City Shale; sc = supercharging; TD = total depth; TOC = top of column; TVDss = true vertical depth subsea.

(Haddad et al., 2012). Nonetheless, these zones are able to withhold substantial subsurface pressures, in the 20,000-psi (1.37×10^5-KPa) range. Laterally extensive shales, regional intraformational seals with significant pressure offsets such as these are noted in many Wilcox wells in the outboard trend of fields such as Great White, Chinook, and St. Malo (Zarra, 2007; Zarra et al., 2019).

Summary of Seal Rock Evaluation, Northern Gulf of Mexico

The examples of Cenozoic and Mesozoic seal rocks cited above are broadly representative of the northern GOM. Without effective seal rocks, the large closures in both the suprasalt and subsalt realm of the deep-water GOM would not have retained the immense volume of discovered hydrocarbons. In many cases, the same age seal rocks also extend to onshore areas as well (Condon et al., 2006; Dyman and Condon, 2006; Pitman et al., 2007). Coastal plain and delta plain or floodplain mudstones also are important seal rocks in onshore regions (Hackley, 2012b; Swanson et al., 2013b; Merrill, 2016), although traps are sometimes smaller given more limited mudstone continuity in nonmarine paleo-environments (Snedden, 2013, 2014). However, it is clear that seal rock capacity, here as offshore, is not simply a function of shale thickness because top seal lithology can vary from silty mudstones to claystones to carbonate-rich shales.

Seal rock failure caused by mechanical breakage of top seals does occur in the northern GOM Basin. These cases are found mainly in offshore areas where elevated crestal pore pressures in reservoirs and seal rocks on the steep flanks of relatively young (Cenozoic) salt-related structures converge on the least principal stress, causing leakage to the surface. However, examples from the supersalt minibasin fields like Mars, Auger, Genesis, and Popeye show that even in these cases, commercial volumes of hydrocarbons can be retained (Seldon and Flemings, 2005).

TRAPS

As discussed in preceding sections, the northern GOM Super Basin has exceptional reservoirs, source rocks, seals, and other supporting elements such as favorable charge histories and salt canopy cooling processes that maintain the Mesozoic source rock viability at depth and out to abyssal plain waters. But without the presence of a diverse set of trap types, it is unlikely that the basin petroleum endowment would have passed the super basin threshold of 5 BOE. Salt tectonics and salt-generated or associated traps make a large part of the trap types. In addition, the long history of exploration would not be possible without such a broad and deep portfolio of trap styles that technology (seismic imaging, drilling, production) has progressively unveiled or made economically feasible.

Analysis of offshore and especially deep-water plays has stressed the important relationship of reservoirs and traps to the extensive salt canopy and compressional fold belts (Figure 17; Weimer et al., 1998, 2016b, 2017a, c; Duncan et al., 2018). Deep-water fields of the northern GOM are located in one of four provinces. (1) Basin province fields lie within salt- or weld-bounded basins formed on the salt canopy. (2) Subsalt province fields lie below the salt canopy or its weld. The subsalt position creates technological challenges both to seismic imaging and drilling. (3) Fold-belt province fields lie along the Mississippi Fan, Keathley–Walker, and Perdido fold belts. (4) Abyssal plain fields lie beneath relatively flat basin floor basinward of the salt and fold belts Weimer et al. (2016b).

Recent drilling into abyssal plain, fold-belt, and subsalt provinces introduced an array of trap configurations rarely penetrated in prior exploration phases (Figure 18). Salt canopies commonly are a major factor, providing both seals and structural discontinuities. Seismic imaging improvements allowed definition of salt-cored folds at the autochthonous salt level (e.g., St. Malo; Figure 18A), autochthonous salt-inverted basins (turtle structures; Figure 18C), and allochthonous salt-cutoff traps and attics (Figure 18E, F). Even subtle traps such as the low-relief closure at the Tiber discovery (Figure 18D) and fault-dependent traps at Hadrian (Figure 18B) are now routinely identified on three-dimensional (3-D) seismic data. More unusual trap styles continue to be delineated and considered for drilling, such as encapsulated minibasins (Figure 18G) and Mesozoic expulsion rollovers such as in the protraction block (e.g., Harding et al., 2016).

Welds may also create traps by juxtaposing different stratigraphic sections and seal where residual

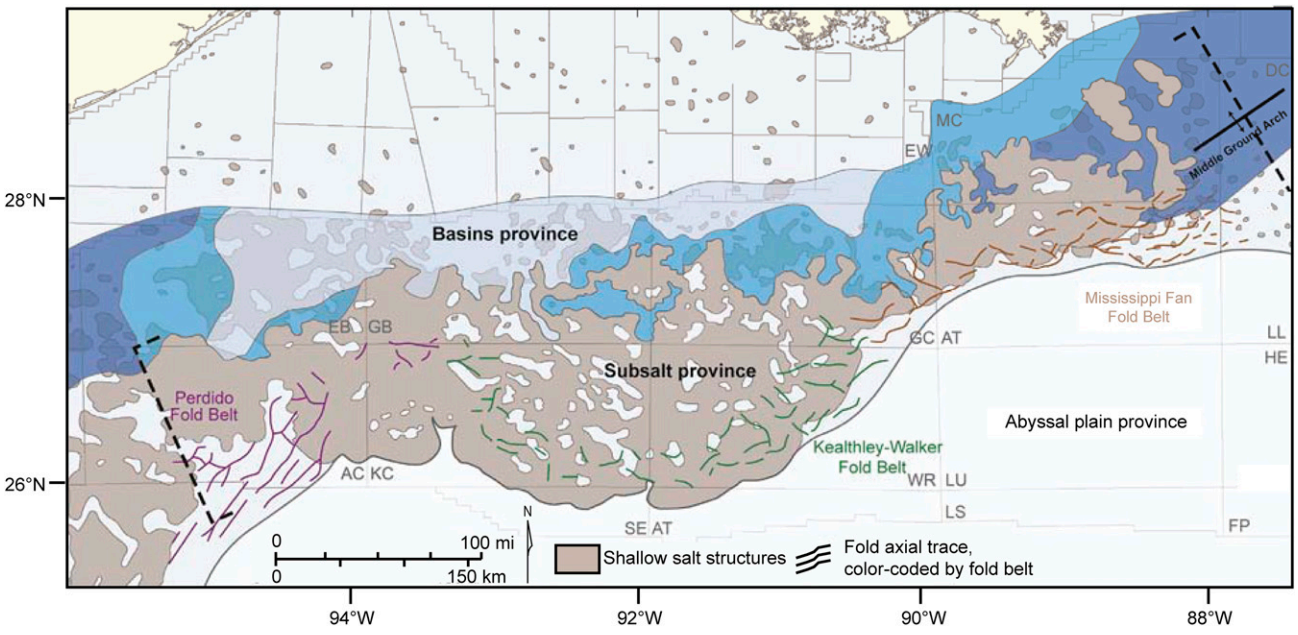

Figure 17. Regional map of the northern Gulf of Mexico shelf and continental slope showing the four major tectonically defined exploration provinces. From Weimer et al. (2016b) and reproduced with permission from the Gulf Coast Association of Geological Societies. Colors indicate age of stratigraphic fill in the Basins province: dark blue = Miocene; medium blue = Pliocene; light blue = Pleistocene. AC = Alaminos Canyon; AT = Atwater Valley; DC = Desoto Canyon; EB = East Breaks; EW = Ewing Bank; FP = Florida Plain; GB = Garden Banks; GC = Green Canyon; HE = Henderson; KC = Keathley Canyon; LL = Lloyd; LS = Lund South; LU = Lund; MC = Mississippi Canyon; SE AT = Sigsbee Escarpment Amery Terrace; WR = Walker Ridge.

or shale gouge is present. Large bucket weld traps (Figure 18H) are common in the central GOM (Figure 17; Pilcher et al., 2011). Megaflaps, steeply dipping stratal packages along sides of diapirs or welds, and other high-relief structures develop from complex salt migration processes (Rowan et al., 2016). Several of these three-way truncation traps hold large columns of oil and gas (e.g., Mount et al., 2019; Wilkins et al., 2019).

Seismic Imaging of the Atlantis Trap: A Success Story

The discoveries and fields mentioned above (e.g., Mars, St. Malo, Appomattox, Cascade) are just a few of the success stories that northern GOM exploration has accumulated since offshore exploration as a whole began in the 1960s and major subsalt deep-water drilling initiated in the early 2000s (Zarra, 2007). Documenting the vast number of successful ventures is beyond the broad scope of this paper. But it is worthwhile considering the impact of advances in seismic imaging and illumination that were a direct result of seismic companies meeting an industry challenge to explore deep below the allochthonous salt canopy.

A case in point is the Atlantis field in the GC protraction block (GC 743; Figure 19, location 19 in Figure 9 and Appendix). Atlantis field is located at the boundary of the fold-belt and abyssal plain provinces (Figure 17). The trap is a relatively simple, deep salt-cored compressional anticline below the allochthonous salt canopy (Mander et al., 2012). Reservoirs are laterally continuous middle Miocene submarine fan deposits with high porosity (26%–32%) and permeability (500–1500 md). The reservoirs exhibit very high net-to-gross ratio and have little clay or cement (Mander et al., 2012).

However, the high quartz content and complex multiphase tectonic history have resulted in localized development of deformation bands and subseismic faults that have induced considerable reservoir compartmentalization (Mander et al., 2012). Deformation bands are known as potential compartment-bounding features in several GOM fields where high net-to-gross sandstone reservoirs are present, including Appomattox (Godo, 2019) and Heidelberg (Mount et al., 2019; Wilkins et al., 2019).

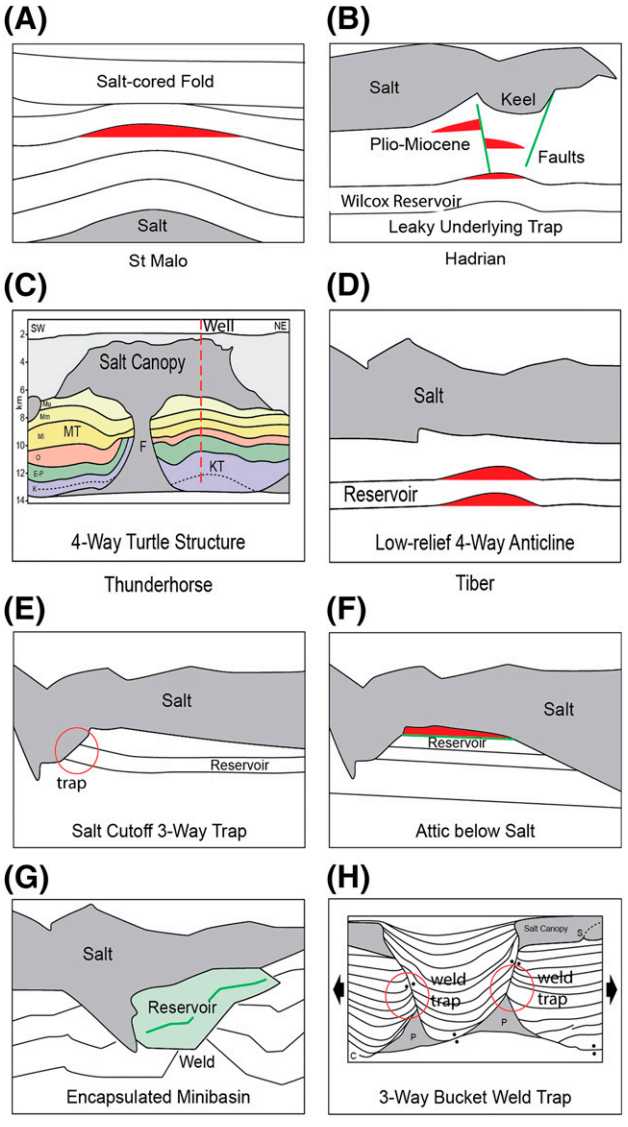

Figure 18. Salt-associated structural trap types of the northern Gulf of Mexico. (A) Buried salt body creating overlying dome. (B) Salt canopy concealing underlying four-way closure with or without faulting. (C) Turtle structures created by salt evacuation around a former withdrawal syncline. Overlying canopy may or may not be present. Subsalt traps include simple and faulted structural closure, turtle structures, and a variety of salt seal configurations. (D) Salt canopy concealing underlying simple four-way closure. (E, F) Salt canopy forming a seal in one or more directions to create trap. (G) Complex salt deformation history resulting in an earlier-formed minibasin fill becoming encapsulated within the salt body and its related welds. (H) Welds on flanks of a primary basin creating updip seal. (E, H) Circles indicate potential traps. From Snedden and Galloway (2019). (C, H) Adapted from Pilcher et al. (2011). C = basal weld; E-P = Eocene–Paleocene; F = salt feeder; K = Cretaceous; KT = Cretaceous turtle; MI = Lower Miocene; Mm = Middle Miocene; Mu = Upper Miocene; MT = Miocene turtle; O = Oligocene; P = salt pedestal; Plio-Miocene = Pliocene–Miocene; S = suture.

Atlantis field is located partially below the allochthonous salt canopy; thus, imaging at deep levels is complicated by the variable salt thickness and significant water depth gradient at the Sigsbee escarpment (Mander et al., 2012). Exploration and development phase 1 3-D seismic data (Figure 20A) were replaced by an isotropic velocity rebuild and reimaging in 2008 (Figure 20B). This improved visualization of the structure and reservoir horizons. Subsequent wide-azimuth, tilted transverse isotropy, and reverse time-migration imaging were completed in 2010 (Figure 20C), which helped reduce reservoir uncertainty for the phase 2 development (Mander et al., 2012). A similar approach, with similar results, was used at the Mad Dog field area (Smith, 2013). Today, wide-azimuth and full-azimuth data are the dominant seismic acquisition technique in the northern and southern GOM Basin. New approaches such as on-bottom node data collection and full-waveform inversion are becoming more commonplace (Fiduk and Lyons, 2019). These and other acquisition, processing, and reimaging improvements have greatly reduced uncertainty in both exploration, development, and production phases (Leyendecker, 2014; Snedden and Galloway, 2019).

Finally, proximity of the northern GOM Basin to Houston, well known as the global center for offshore facilities design, drilling, and petroleum geoscience technology, should be noted. The numerous commercial research laboratories here have hosted development of a wide range of technologies from 3-D and four-dimensional seismic data, sequence stratigraphy, subsea completions, tension-leg platforms, frac-pack completions, and many other innovative approaches to exploration, development, and production.

SUMMARY: INSIGHTS FROM THE NORTHERN GULF OF MEXICO SUPER BASIN FOR OTHER BASINS

It is useful to consider the broad insights that might be garnered from a super basin like the northern GOM. Some lessons are unique to the northern GOM Basin and some are relevant basin-wide, whereas other insights may have global applicability. These pertain to reservoirs, source rocks, seal rocks, charge history, and trap development, which are all the elements that make

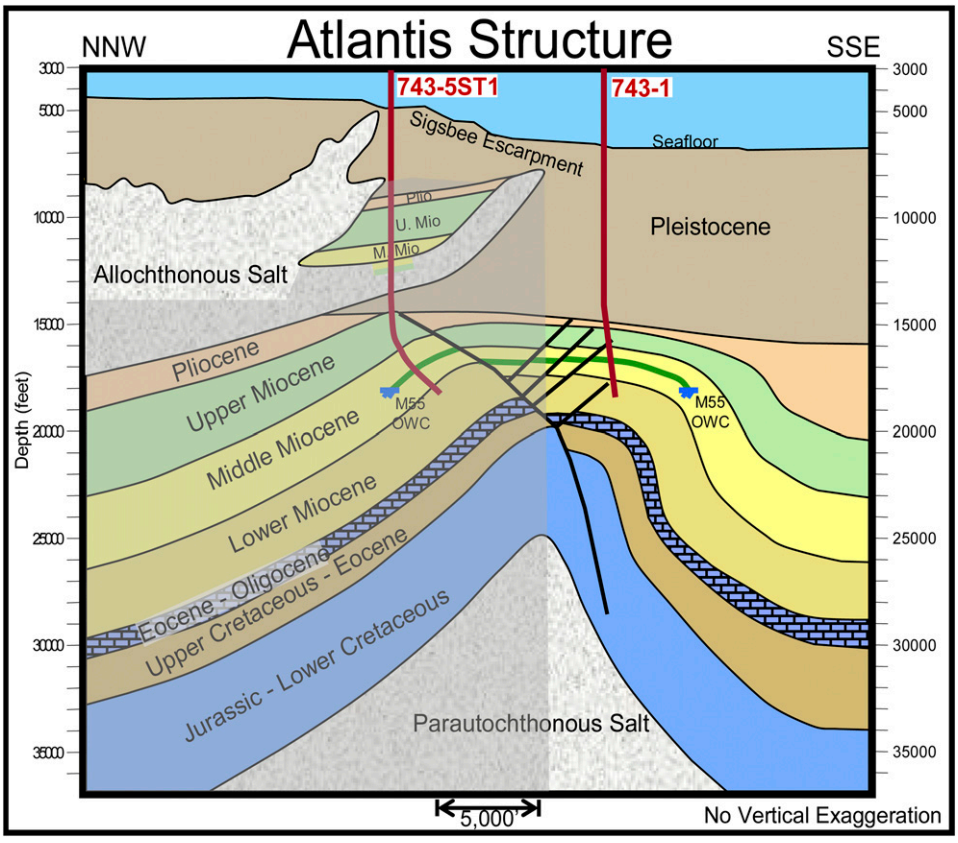

Figure 19. Structural cross section of the Atlantis field, which lies partially below the allochthonous salt canopy. Middle (M.) Miocene (Mio) reservoirs are lobe deposits of a submarine fan system fronting the slope apron of the Tennessee delta system. Transparent gray area shows the low seismic illumination area below salt that obscures interpretation. From Mander et al. (2012). M55 = Miocene Zone 55; OWC = oil-water contact; Plio = Pliocene; ST1 = sidetrack 1; U. = Upper.

up an efficient, formidable world-class petroleum system.

To generate sufficient gross sandstone rock volume and a regional stacking of porous zones that constitute the hallmark of a super basin, a well-defined pathway from source terranes to depositional sink must be evident or at least inferred from tectonic reconstructions. In the case of the northern GOM Basin, prominent mountain belts were formed, exposed, and eroded over multiple structural events and paleoclimatic phases since the basin formed (Galloway et al., 2011; Snedden et al., 2018). The Cordilleran and Laramide orogens were the largest volumetric contributors for the Cenozoic, but the extant Appalachian tectonic highlands in the Mesozoic and associated rejuvenated plateaus in the Miocene were also significant catchments during the Miocene (Boettcher and Milliken, 1994). These high rates of Cenozoic deposition on a mobile salt substrate also were a key factor in generating a diverse portfolio of salt tectonic structures and trap types. Relatively late Cenozoic burial, in comparison to other global basins, also improved charge–trap timing relationships.

Carbonate reservoirs, which are so important in the Mesozoic section of the onshore northern GOM and southern GOM, mainly require stable platforms; warm, equitable climates; and low-turbidity water to develop grainstone banks, thrombolytic buildups, platform margin reefs, and associated grainstone aprons. In addition, favorable postdepositional and burial diagenetic processes allow development of economic levels of porosity and permeability. Evidence from extensive drilling shows that all these depositional processes worked in the northern GOM.

Seal rocks also were formed during many of these depositional events and stratigraphic sequences. Given the large hydrocarbon endowment, seal rock quality is obviously sufficient in many intervals to resist both capillary and mechanical leakage over long

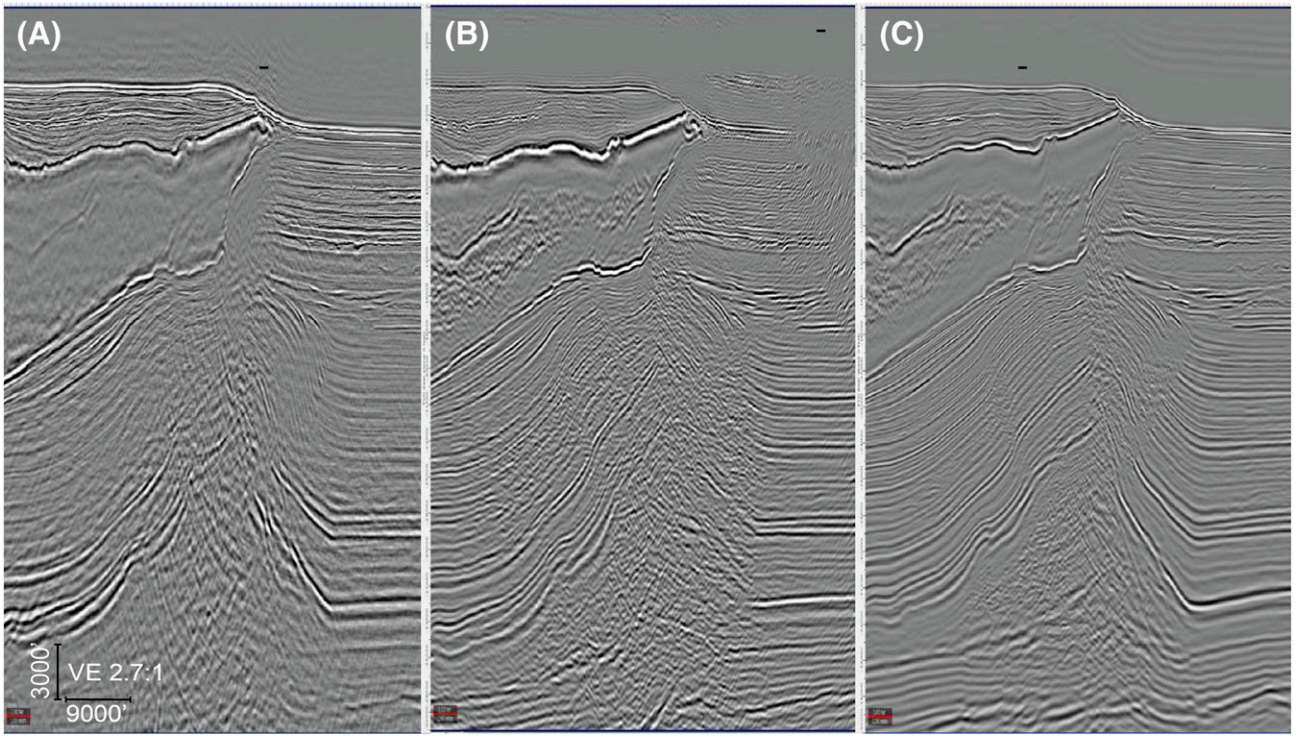

Figure 20. Example of imaging improvement with wide-azimuth (WAZ) seismic data below the salt canopy in the northern Gulf of Mexico, Atlantis field area. (A) Narrow azimuth towed streamer (NATS) (2003). (B) On-bottom node (OBN) WAZ, isotropic SM (2008). (C) OBN WAZ and NATS merge, tilted transverse isotropy reverse time migration (2010). From Mander et al. (2012). SM = seismic modeling; VE = vertical exaggeration.

geologic durations. Seal rocks are both stratigraphically and geographically widespread, a distribution reflecting allogenic processes (e.g., relative sea-level changes resulting in development of regional or global transgressions) and autogenic processes (e.g., submarine channel avulsion, fan abandonment, etc.).

Source rock occurrence, which includes organic production, preservation, maturation, migration, and appropriate timing relative to trap development, is optimized in the basin for a variety of reasons. Global OAEs were a facilitating factor, but basin-specific processes related to structural and paleogeographic restriction, salinity stratification, and reduced oxygen levels enhanced source rock quality so that at least two world-class source horizons (Cenomanian–Turonian and Tithonian centered) are present, with significant additions from the Jurassic Oxfordian, Paleogene, and other intervals. Multiple working source rocks ensure that failure cases of underfilled or wet traps caused by source inefficiency are relatively rare here.

The role of salt, particularly the allochthonous salt canopy, in enlarging the basin hydrocarbon endowment cannot be overestimated. The emergence of the prolific subsalt play in the deep-water northern GOM reflects reduced heat flow, delayed maturation, and relatively recent migration from deeply buried Mesozoic source rocks into traps formed by salt tectonics.

Salt tectonics occurred over a long time frame, from early basin formation to near present day. This provides a wide diversity of trap types, but also an extended exploration history as plays matured from the hunt for simple diapiric traps, to the search for deep salt-cored compressional folds, bucket welds, and other complex tectonic configurations.

Paralleling and clearly driving this expanding portfolio of salt tectonic traps in the northern GOM is the increased sophistication of seismic acquisition, processing, and interpretation. Other basins with prominent salt bodies (e.g., Brazil, Caspian Basin, etc.) have undoubtedly benefited from major technical advances initiated to support industry activity in the GOM. This also applies to improvements in deep, high-pressure, high-temperature drilling, logging, and production in ultra–deep-water regimes.

The northern GOM Super Basin should be considered as a natural laboratory for illustrating the remarkable individual elements of a petroleum system but also the favorable confluence of these elements to yield one of the largest hydrocarbon endowments in the world. The macroeconomics of the basin, as they relate to market access, lease, and royalty terms, and so forth, obviously are a factor in its success. But these would not be relevant unless the underlying oil and gas commodity prize is available and in sufficient quantity to ensure that exploration, development, and production efforts can weather the ups and downs of past, current, and future supply–demand cycles.

APPENDIX

Table 2. Key Well Identification and Location Information

Number	Figure Number or Text	Longitude, °	Latitude, °	Operator	Lease/Block/Prospect	API Number
1	9	−94.502843	30.412557	Black Stone Minerals	A-318-1	421993311900
2	Text	−94.51757	26.408956	Shell	AC 557-1 BAHA II	608054001302
3	9	−89.623772	27.768949	Chevron	AT 182-1 Sturgis	608184004201
4	9	−88.569107	27.63986	Burlington Resources	AT 336-1 Showboat	608184001200
5	9	−88.373108	27.556494	Eni	AT 428-2 Tembo	608184007201
6	6	−87.832326	28.802492	Murphy	DC 178-1 Titan	608234002700
7	6	−87.685255	28.714777	Shell	DC 269-1 Shiloh	608234000600
8	6	−87.817913	28.488355	Shell	DC 486-1 Fredericksburg	608234001500
9	6	−87.961916	28.460289	Shell	DC 525-1 Rydberg	608174128000
10	6, 10	−87.898985	28.444485	Shell	DC 529-1 Petersburg	608234002100
11	6	−87.598474	28.461494	Anadarko	DC 535-1 Raptor	608234002001
12	6	−86.869774	28.273252	BHP	DC 726-2 Sake II	608234002400
13	6	−87.507759	28.221337	Marathon	DC 757-1 Madagascar	608234002500
14	9	−87.776193	28.054909	Kerr-McGee	DC 927-1	608234000500
15	7A	−87.843536	28.585154	Shell	DC 398-1 Gettysburg	608234002800
16	7D	−94.875582	27.034761	Exxon	EB 946-1 Diana-3	608044016300
17	11	−89.945892	28.070778	Amerada-Hess	EW 922-1 Wrigley	608105008700
18	11, 12	−93.641561	27.216432	Amerada-Hess	GB 754-1 Norton	608074065300
19	19	−90.029239	27.227952	BP	GC 743-1 Atlantis	608114027700
20	19	−90.032866	27.249338	BP	GC 743-5 Atlantis ST1	608114034900
21	12	−93.269044	26.878318	BP	KC 102-1 Tiber	608084001500
22	Text	−92.911791	26.299191	Unocal	KC 681-1 Sardinia	608084000500
23	6	−87.765137	27.544156	Shell	LL 399-1 Cheyenne	608244000303
24	Text	−89.94912	21.450546	IODP	M0077 borehole	NA
25	6, 17	−87.996745	28.605245	Shell	MC 392-1 Appomattox	608174117203
26	6, 12	−87.996764	28.610131	Shell	MC 392-1 Appomattox ST-2	608174117202
27	6	−88.247965	28.367001	Chevron	MC 607-1 Ballymore	608174135800
28	Text	−87.973659	28.919307	PXP	MC 84-1 King	608174043170
29	14, 15	−87.982175	28.634414	Shell	MC 348-3 Appomattox Northwest	608174119300
30	14, 15	−88.026333	28.617993	Shell	MC 391-1 Appomattox Southwest	608174120500
31	6	−88.088649	28.422162	Shell	MC 566-1 Fort Sumter	608174131801
32	12	−90.533168	31.1507	Sun Oil	W. P. Spinks-1	231132002000
33	16	−90.490171	26.733803	Murphy	WR 250-CA004 Cascade	608124004701

Abbreviations: AC = Austin Chalk; AT = Atwater Valley; DC = Desoto Canyon; GB = Garden Banks; GC = Green Canyon; EB = East Breaks; EW = Ewing Bank; IODP = International Ocean Drilling Project; KC = Keathley Canyon; LL = Lloyd; MC = Mississippi Canyon; NA = not available; WR = Walker Ridge.

REFERENCES CITED

Aplin, A. C., and S. R. Larter, 2005, Fluid flow, pore pressure, wettability, and leakage in mudstone cap rocks, *in* P. Boult and J. Kaldi, eds., Evaluating fault and cap rock seals: AAPG Hedberg Series 2, p. 1–12.

Barboza-Gudiño, J. R., A. Zavala-Monsiváis, G. Venegas-Rodríguez, and L. D. Barajas-Nigoche, 2010, Late Triassic stratigraphy and facies from northeastern Mexico: Tectonic setting and provenance: Geosphere, v. 6, 621–640, doi:10.1130/GES00545.1.

Blanke, S. J., L. C. Meibos, and P. S. Kline, 2009, A seismically defined ancient anoxic intraslope basin in Hardin County, Texas—Potential source and seismic pitfall: Gulf Coast Association of Geological Societies Transactions, v. 59, p. 87–99.

Blum, M., and M. Pecha, 2014, Mid-Cretaceous to Paleocene North American drainage reorganization from detrital zircons: Geology, v. 42, no. 7, p. 607–610, doi:10.1130/G35513.1.

Boettcher, S. S., and K. L. Milliken, 1994, Mesozoic-Cenozoic unroofing of the Southern Appalachian Basin: Apatite fission track evidence from Middle Pennsylvanian sandstones: Journal of Geology, v. 102, no. 6, p. 655–668, doi:10.1086/629710.

Bouma, A. H., 1962, Sedimentology of some Flysch deposits: A graphic approach to facies interpretation: Amsterdam, Elsevier, 168 p.

Brown, A., 2003, Improved interpretation of wireline pressure data: AAPG Bulletin, v. 87, no. 2, p. 295–311.

Bureau of Ocean Energy Management, 2017, Assessment of technically and economically recoverable hydrocarbon resources of the Gulf of Mexico Outer Continental Shelf as of January 1, 2014: Washington, DC, Bureau of Ocean Energy Management Outer Continental Shelf Report 2017–005, 50 p.

Cantú-Chapa, A., 2009, Upper Jurassic stratigraphy (Oxfordian and Kimmeridgian) in petroleum wells of the Campeche shelf, Gulf of Mexico, *in* C. Bartolini and J. R. Román Ramos eds., Petroleum systems in the southern Gulf of Mexico: AAPG Memoir 90, p. 79–91, doi:10.1306/13191079M902804.

Chen, A., 2014, The practice of graphical fluid-gradient interpretations of formation tester pressure data: AAPG Bulletin, v. 98, no. 7, p. 1431–1448, doi:10.1306/12101313122.

Cicero, A. D., I. Steinhoff, T. McClain, K. A. Koepke, and J. D. Dezelle, 2010, Sequence stratigraphy of the Upper Jurassic mixed carbonate/siliciclastic Haynesville and Bossier shale depositional systems in east Texas and northern Louisiana: Gulf Coast Association of Geological Societies Transactions, v. 60, p. 133–148.

Claypool, G. E., and E. A. Mancini, 1989, Geochemical relationships of petroleum in Mesozoic reservoirs to carbonate source rocks of Jurassic Smackover Formation, southwestern Alabama: AAPG Bulletin, v. 73, no. 7, p. 904–924.

Cole, G., A. Yu, F. Peel, R. Requejo, J. DeVay, J. W. Brooks, B. Bernard, J. Zumberge, and S. Brown, 2001, Constraining source and charge risk in deepwater areas: World Oil, v. 222, no. 10, p. 69–77.

Cole, G. A., A. G. Requejo, A. Yu, J. DeVay, C. Taylor, P. Dougherty, F. Peel et al., 1999, The geochemical and basin modeling aspects of the Jurassic to Lower Cretaceous sourced petroleum system, deepwater to ultra-deepwater Gulf of Mexico, offshore Louisiana: Tercera Conferencia Internacional Conjunta Asociación Mexicana de Geólogos Petroleros/AAPG, Veracruz, Mexico, October 10–13, 1999, 8 p.

Comet, P. A., 1992, Maturity mapping of northern Gulf of Mexico oils using biomarkers: Gulf Coast Association of Geological Societies Transactions, v. 42, p. 433–448.

Comet, P. A., J. K. Rafalska, and J. M. Brooks, 1993, Sterane and triterpene patterns as diagnostic tools in the mapping of oils, condensates, and source rocks of the Gulf of Mexico region: Organic Geochemistry, v. 20, no. 8, p. 1265–1296, doi:10.1016/0146-6380(93)90014-3.

Condon, S. M., T. S. Dyman, T. R. Klett, P. A. Le, and L. R. H. Biewick, 2006, Petroleum systems and geologic assessment of undiscovered oil and gas, Navarro and Taylor Groups, Western Gulf Province, Texas: Reston, Virginia, US Geological Survey Data Series 69-H, 76 p.

Cox, R. T., and R. B. Van Arsdale, 2002, The Mississippi Embayment, North America: A first order continental structure generated by the Cretaceous superplume mantle event: Journal of Geodynamics, v. 34, no. 2, p. 163–176, doi:10.1016/S0264-3707(02)00019-4.

Cunningham, R., M. Purkey-Phillips, J. W. Snedden, I. O. Norton, C. M. Lowery, J. W. Virdell, and C. D. Barrie, in press, Paleocene-Eocene paleoenvironmental evolution of the Northern Gulf of Mexico: Impact on organic carbon sequestration: Paleoceanography and Paleoclimatology.

Cunningham, R., J. W. Snedden, I. O. Norton, H. C. Olson, T. L. Whiteaker, and J. W. Virdell, 2016, Upper Jurassic Tithonian-centered source mapping in the deepwater northern Gulf of Mexico: Interpretation, v. 4, no. 1, p. SC97–SC123, doi:10.1190/INT-2015-0093.1.

Dawson, W. C., and W. R. Almon, 2005, Shale facies variability and sequence stratigraphy: Application to top seal prediction in deepwater depositional systems: Gulf Coast Association of Geological Societies Transactions, v. 55, p. 133–145.

DeCelles, P. G., 2004, Late Jurassic to Eocene evolution of the Cordilleran thrust belt and foreland basin system, western U.S.A.: American Journal of Science, v. 304, no. 2, p. 105–168, doi:10.2475/ajs.304.2.105.

de Lourdes Clara Valdés, M., L. Villanueva Rodríguez, and E. Caballero García, 2009, Geochemical integration and interpretation of source rocks, oils, and natural gases in southeastern Mexico, *in* C. Bartolini and J. R. Román Ramos, eds., Petroleum systems in the southern Gulf of Mexico: AAPG Memoir 90, p. 337–368, doi:10.1306/13191091M903337.

Denne, R. A., E. D. Scott, D. P. Eickhoff, J. A. Kaiser, R. J. Hill, and J. M. Spaw, 2013, Massive Cretaceous-Paleogene boundary deposit, deep-water Gulf of Mexico: New evidence for widespread Chicxulub-induced slope failure: Geology, v. 41, no. 9, p. 983–986.

Downey, M. W., 1984, Evaluating seals for hydrocarbon accumulations: AAPG Bulletin, v. 68, no. 11, p. 1752–1763.

Duncan, T., B. I. Braathen, N. McCormack, M. Stauble, L. Campbell, M. Cizek, S. Rasmussen, S. Khurana, and J. Wilson, 2018, One Gulf reaching 50 billion BOE and growing: Offshore Technology Conference, Houston, Texas, April 30–May 3, 2018, OTC-29074-MS, 24 p.

Dyman, T. S., and S. M. Condon, 2006, Assessment of undiscovered conventional oil and gas resources–Upper Jurassic-Lower Cretaceous Cotton Valley group, Jurassic Smackover interior salt basins total petroleum system, in the East Texas basin and Louisiana-Mississippi salt basins provinces: Reston, Virginia, US Geological Survey Digital Data Series 69-E-2, 52 p.

Eikrem, V., R. Li, M. Medeiros, B. J. McKee, B. L. Boswell, E. E. Shumilak, and R. Mohan, 2010, SS: Perdido development project: Great White WM12 reservoir and Silvertip M. Frio field development plans and comparison of recent well results with pre-drill models: Offshore Technology Conference, Houston, Texas, May 3–6, 2010, OTC-20879-MS, 10 p., doi:10.4043/20879-MS.

Enomoto, C. B., K. R. Scott, B. J. Valentine, P. C. Hackley, K. Dennen, and C. D. Lohr, 2012, Preliminary evaluation of the shale gas prospectivity of the Lower Cretaceous Pearsall Formation in the onshore Gulf Coast region: Gulf Coast Association of Geological Societies Transactions, v. 62, p. 93–115.

Ewing, T. E., 2009, The ups and downs of the Sabine Uplift and the northern Gulf of Mexico Basin: Jurassic basement blocks, Cretaceous thermal uplifts, and Cenozoic flexure: Gulf Coast Association of Geological Societies Transactions, v. 59, p. 253–269.

Ewing, T. E., 2016, Texas through time: Lone Star geology, landscapes, and resources: Austin, Texas, The University of Texas Bureau of Economic Geology Udden Series 6, 431 p.

Ewing, T. E., and W. E. Galloway, 2019, Evolution of the northern Gulf of Mexico sedimentary basin, *in* A. D. Miall, ed., The sedimentary basins of the United States and Canada, 2nd ed.: Amsterdam, Elsevier, p. 627–694, doi: 10.1016/B978-0-444-63895-3.00016-4.

Ferworn, K., J. Zumberge, and S. Brown, 2003, Integration of geochemistry and reservoir fluid properties: Bureau of Economic Geology Petroleum Technology Transfer Council Workshop, First Annual Fluids Symposium Reservoir Fluids 2003: PVT and Beyond: Lafayette, Louisiana, June 25, 2003, 51 p.

Fiduk, C., and K. Lyons, 2019, Evolution of marine seismic imaging from late 1990s to middle 2010s: A WesternGeco perspective, *in* J. C. Fiduk and N. C. Rosen, eds., Salt tectonics, associated processes, and exploration potential: Revisited: 1989–2019: 37th Annual Gulf Coast Section of SEPM Perkins-Rosen Research Conference, Houston, Texas, December 3–6, 2019, p. 1–19.

Fryklund, B., and P. Stark, 2016, Super basins – The basins that keep on giving, accessed February 1, 2020, https://ihsmarkit.com/solutions/permian-basin.html.

Galloway, W. E., 2008, Depositional evolution of the Gulf of Mexico sedimentary basin, *in* A. D. Miall, ed., The sedimentary basins of the United States and Canada: Amsterdam, Elsevier, v. 5, p. 505–549.

Galloway, W. E., T. L. Whiteaker, and P. E. Ganey-Curry, 2011, History of Cenozoic North American drainage basin evolution, sediment yield, and accumulation in the Gulf of Mexico basin: Geosphere, v. 7, no. 4, p. 938–973, doi: 10.1130/GES00647.1.

Godo, T., 2017, The Appomattox field: Norphlet Aeolian sand dune reservoirs in the deep-water Gulf of Mexico, *in* R. K. Merrill and C. A. Sternbach, eds., Giant fields of the decade 2000–2010: AAPG Memoir 113, p. 29–54, doi:10.1306/13572000M1133680.

Godo, T., 2019, The Smackover-Norphlet petroleum system, deepwater Gulf of Mexico: Oil fields, oil shows, and dry holes: Gulf Coast Association of Geological Societies Journal, v. 8, p. 104–152.

González-Garcia, R., and N. Holguín-Quiñones, 1992, Las Rocas generadoras de Mexico: Boletín AMGP, articulo reeditado del, XLII, 16–30.

Guzman-Vega, M. A., 2000, Origin of petroleum in the Mexican Gulf Coast basin, 2000 (abs.): Gulf Coast Association of Geological Societies Transactions of the 50th Annual Convention, Houston, Texas, October 25–27, 2000, 1 p.

Guzmán-Vega, M. A., L. Castro Ortíz, J. R. Román-Ramos, L. Medrano-Morales, L. C. Valdéz, E. Vázquez-Covarrubias, and G. Ziga-Rodríguez, 2001, Classification and origin of petroleum in the Mexican Gulf Coast Basin: An overview, *in* C. Bartolini, R. T. Buffler, and A. Cantú-Chapa, eds., The western Gulf of Mexico Basin: Tectonics, sedimentary basins, and petroleum systems: AAPG Memoir 75, p. 127–142.

Guzman-Vega, M. A., and M. R. Mello, 1999, Origin of oil in the Sureste Basin, Mexico: AAPG Bulletin, v. 83, no. 7, p. 1068–1095.

Hackley, P. C., 2012a, Geologic assessment of undiscovered conventional oil and gas resources—Middle Eocene Claiborne Group, United States part of the Gulf of Mexico Basin: Reston, Virginia, US Geological Survey Open-File Report 2012-1144, 87 p., doi:10.3133/ofr20121144.

Hackley, P. C., 2012b, Geological and geochemical characterization of the Lower Cretaceous Pearsall Formation, Maverick Basin, south Texas: A future shale gas resource?: AAPG Bulletin, v. 96, no. 8, p. 1449–1482, doi:10.1306/11221111071.

Hackley, P. C., K. O. Dennen, R. M. Gesserman, and J. L. Ridgley, 2009, Preliminary vitrinite and bitumen reflectance, total organic carbon, and pyrolysis data for samples from Upper and Lower Cretaceous strata, Maverick Basin, south Texas: Reston, Virginia, US Geological Survey Open-File Report 2009-1220, 3 p., accessed October 5, 2020, https://pubs.usgs.gov/of/2009/1220/.

Haczewski, G., 1976, Sedimentological reconnaissance of the San Cayetano Formation: An accumulative continental margin in the Jurassic of western Cuba: Acta Geologica Polonica, v. 26, no. 2, p. 331–353.

Haddad, Z., M. B. Smith, and F. Dias De Moraes, 2012, Designing multistage frac packs on the Lower Tertiary Formation–Cascade and Chinook Project: SPE Drilling and Completion, v. 27, no. 1, SPE-140498-PA, 15 p.

Hammes, U., R. Eastwood, G. McDaid, E. Vankov, S. A. Gherabit, K. Smye, J. Shultz, E. Potter, S. Ikonnikova, and S. Tinker, 2016, Regional assessment of the Eagle Ford Group of South Texas, USA: Insights from lithology, pore volume, water saturation, organic richness, and productivity correlations: Interpretation, v. 4, no. 1, p. SC125–SC150, doi:10.1190/INT-2015-0099.1.

Hammes, U., H. S. Hamlin, and T. E. Ewing, 2011, Geologic analysis of the Upper Jurassic Haynesville Shale in east Texas and west Louisiana: AAPG Bulletin, v. 95, no. 10, p. 1643–1666, doi:10.1306/02141110128.

Harding, A., L. Walker, S. Ehlinger, and T. Chapman, 2016, The siliciclastic Upper Cretaceous play of eastern Mississippi Canyon, *in* C. M. Lowery, J. W. Snedden, and N. C. Rosen, eds., Mesozoic of the Gulf Rim and beyond: New progress in science and exploration of the Gulf of Mexico: 35th Annual Gulf Coast Section of the SEPM Foundation Perkins-Rosen Research Conference, Houston, Texas, December 7–9, 2016, p. 215-231.

Henry, L. C., J. A. Wadsworth, and B. Hansen, 2017, Visualizing a sub-salt field with image logs: Image facies, mass transport complexes, and reservoir implications from Thunder Horse, Mississippi Canyon, Gulf of Mexico: AAPG Search and Discovery article 10938, accessed April 7, 2020, http://www.searchanddiscovery.com/documents/2017/10938henry/ndx_henry.pdf.

Hentz, T. F., and S. C. Ruppel, 2011, Regional stratigraphic and rock characteristics of Eagle Ford Shale in its play area: Maverick Basin to East Texas Basin: Gulf Coast Association of Geological Societies Transactions, v. 60, p. 325–337.

Hentz, T. F., S. Seni, E. G. Wermund, B. Harder, B. Jones, T. Tremblay, and D. Salazar, 1997, Atlas of Northern Gulf of Mexico gas and oil reservoirs: Volume 2. Pliocene and Pleistocene reservoirs: Austin, Texas The University of Texas at Austin Bureau of Economic Geology, 78 p.

Hentz, T. F., and H. Zeng, 2003, High-frequency Miocene sequence stratigraphy, offshore Louisiana: Cycle framework and influence on production distribution in a mature shelf province: AAPG Bulletin, v. 87, no. 2, p. 197–230, doi:10.1306/09240201054.

Holguín-Quiñones, N., J. M. Brooks, J. R. Román-Ramos, B. B. Bernard, J. Lara-Rodríguez, J. E., Zumberge, L. Medrano-Morales et al., 2005, Estudio regional de manifestaciones superficiales de aceite y gas en el Sur del Golfo de México, su origen e implicationes exploratorias: Boletín de la Asociación Mexicana de Geólogos Petroleros, v. 52, no. 1, p. 20–41.

Hood, K. C., L. M. Wenger, O. P. Gross, and S. C. Harrison, 2002, Hydrocarbon systems analysis of the northern Gulf of Mexico: Delineation of hydrocarbon migration pathways using seeps and seismic imaging, *in* D. Schumacher and L. A. LeSchack, eds., Surface exploration case histories: Applications of geochemistry, magnetics, and remote sensing: AAPG Studies in Geology 48 and Society of Exploration Geophysicists Geophysical References Series 11, p. 25–40.

Hudec, M. R., M. P. A. Jackson, and F. J. Peel, 2013, Influence of deep Louann structure on the evolution of the northern Gulf of Mexico: AAPG Bulletin, v. 97, no. 10, p. 1711–1735, doi:10.1306/04011312074.

Hull, D., 2011, Stratigraphic architecture, depositional systems, and reservoir characteristics of the Pearsall shale-gas system, Lower Cretaceous, South Texas, Master's thesis, The University of Texas at Austin, Austin, Texas, 208 p.

Hull, D., B. Loucks, and K. Milliken, 2012, Lower Cretaceous Pearsall oceanic anoxic events and associated development of shale-gas reservoirs in South Texas: AAPG Search and Discovery article 80240, accessed October 4, 2020, http://www.searchanddiscovery.com/pdfz/documents/2012/80240hull/ndx_hull.pdf.html.

Hunt, B., D. Robinson, A. L. Weislogel, and R. C. Ewing, 2017, Sediment source regions and paleotransport of the Upper Jurassic Norphlet Formation, eastern Gulf of Mexico: AAPG Bulletin, v. 101, no. 9, p. 1519–1542, doi:10.1306/10171615156.

Husson, L., X. Le Pichon, P. Henry, N. Flotte, and C. Rangin, 2008, Thermal regime of the NW shelf of the Gulf of Mexico Part B: Heat flow: Bulletin de la Société Géologique de France, v. 179, no. 2, p. 139–145, doi:10.2113/gssgfbull.179.2.139.

Jarvie, D. M., A. Morelos, J. Reed, M. Tobey, and H. Alim, 2004, Geochemical characteristics of Tertiary, Cretaceous, and Jurassic source rocks, Gulf of Mexico (abs.): AAPG International Conference, Cancun, Mexico, October 24–27, 2004, accessed July 5, 2016, http://www.searchanddiscovery.com/pdfz/documents/abstracts/2004intl_cancun/short/A90112.pdf.html.

Jenkyns, H. C., 2010, Geochemistry of oceanic anoxic events: Geochemistry, Geophysics, Geosystems, v. 11, no. 3, 30 p., doi:10.1029/2009GC002788.

Jennings, J. B., 1987, Capillary pressure techniques: Application to exploration and development geology: AAPG Bulletin, v. 71, no. 10, p. 1196–1209.

Katz, B. J., 1984, Source quality and richness of Deep Sea Drilling Project site 535 sediments, southeastern Gulf of Mexico, *in* R. Buffer, W. Schlager, and K. A. Pisciotto, eds., Initial reports of the Deep Sea Drilling Project: Washington, DC, US Government Printing Office, v. 77, p. 445–450, doi:10.2973/dsdp.proc.77.111.1984.

Klemme, H. D., and G. F. Ulmishek, 1991, Effective petroleum source rocks of the world: Stratigraphic distribution and controlling depositional factors: AAPG Bulletin, v. 75, no. 12, p. 1809–1851.

Kosters, E. C., and R. J. Finley; Gas Research Institute, 1989, Atlas of major Texas gas reservoirs: Austin, Texas, The University of Texas at Austin Bureau of Economic Geology, 161 p.

Lawton, T. F., J. E. Ruiz-Uruena, L. A. Solari, C. Tarango Terrazas, E. Juárez-Arriaga, and C. Ortega-Obregón, 2018, Provenance of Upper Triassic–Middle Jurassic strata of the Plomosas uplift, east-central Chihuahua, Mexico, and possible sedimentologic connections with Colorado Plateau depositional systems, *in* R. V. Ingersoll, T. F. Lawton, and S. A. Graham, eds., Tectonics, Sedimentary Basins, and Provenance: A celebration of the career of William R. Dickinson: Geological Society of America

Special Paper 540, p. 481–507, doi:10.1130/2018.2540(22).
Leyendecker, E. A., 2014, The Gulf of Mexico advantage: AAPG Search and Discovery article 110175, accessed October 4, 2020, http://www.searchanddiscovery.com/documents/2014/110175leyendecker/ndx_leyendecker.pdf.
Lowery, C. M., T. J. Bralower, J. D. Owens, F. J. Rodríguez-Tovar, H. Jones, J. Smit, M. T. Whalen et al., 2018, Rapid recovery of life at ground zero of the end-Cretaceous mass extinction: Nature, v. 558, no. 7709, p. 288–291, doi:10.1038/s41586-018-0163-6.
Lowery, C. M., R. Cunningham, C. D. Barrie, T. J. Bralower, and J. W. Snedden, 2017, The northern Gulf of Mexico during OAE2 and the relationship between water depth and black shale development: Paleoceanography and Paleoclimatology, v. 32, no. 12, p. 1316–1335, doi:10.1002/2017PA003180.
Lu, J., K. Milliken, R. M. Reed, and S. Hovorka, 2011, Diagenesis and sealing capacity of the middle Tuscaloosa mudstone at the Cranfield carbon dioxide injection site, Mississippi, U.S.A.: Environmental Geoscience, v. 18, no. 1, p. 35–53, doi:10.1306/eg.09091010015.
Magoon, L. B., T. L. Hudson, and H. E. Cook, 2001, Pimienta-Tamabra(!)—A giant supercharged petroleum system in the southern Gulf of Mexico, onshore and offshore Mexico, *in* C. Bartolini, R. T. Buffler, and A. Cantú-Chapa, eds., The western Gulf of Mexico Basin: Tectonics, sedimentary basins, and petroleum systems: AAPG Memoir 75, p. 83–125, doi:10.1306/M75768C4.
Mancini, E. A., J. C. Llinás, W. C. Parcell, M. Aurell, B. Bádenas, R. R. Leinfelder, and D. J. Benson, 2004, Upper Jurassic thrombolite reservoir play, northeastern Gulf of Mexico: AAPG Bulletin, v. 88, no. 11, p. 1573–1602, doi:10.1306/06210404017.
Mancini, E. A., R. M. Mink, B. L. Bearden, and R. P. Wilkerson, 1985, Norphlet Formation (Upper Jurassic) of southwestern and offshore Alabama: Environments of deposition and petroleum geology: AAPG Bulletin, v. 69, no. 6, p. 881–898.
Mancini, E. A., B. H. Tew, and R. M. Mink, 1992, Hydrocarbon productivity characteristics of Upper Jurassic Smackover carbonates, eastern Gulf Coastal Plain: Gulf Coast Association of Geological Societies Transactions, v. 42, p. 237–244.
Mander, J., J. d'Ablaing, J. Howie, K. Wells, R. Ramazanova, D. Shepherd, and C. Lee, 2012, 21st century Atlantis–Incremental knowledge from a staged-approach to development, illustrated by a complex deep-water field, *in* N. C. Rosen, P. Weimer, S. M. Coutes dos Anjos, S. Henrickson, E. Marques, M. Mayall, R. Fillon, et al., eds., New understanding of the petroleum systems of continental margins of the world: Houston, Texas, Gulf Coast Section of the Society for Sedimentary Geology 32, p. 65–95.
Mankiewicz, P. J., R. J. Pottorf, M. G. Kozar, and P. Vrolijk, 2009, Gas geochemistry of the Mobile Bay Jurassic Norphlet Formation: Thermal controls and implications for reservoir connectivity: AAPG Bulletin, v. 93, no. 10, p. 1319–1346, doi:10.1306/05220908171.
Marchand, A. M. E., G. Apps, W. Li, and J. R. Rotzien, 2015, Depositional processes and impact on reservoir quality in deepwater Paleogene reservoirs, US Gulf of Mexico: AAPG Bulletin, v. 99, no. 9, p. 1635–1648, doi:10.1306/04091514189.
Mattos, D. M., C. L. Palagi, O. J. S. Ribeiro, and S. da Matta Jr., 2013, Development and production of Cascade and Chinook fields in the Gulf of Mexico: An overview: Offshore Technology Conference, Houston, Texas, May 6–9, 2013, OTC-24156-MS, 13 p.
Meckel, L. D. III, G. A. Ugueto, H. D. Lynch, E. W. Cumming, B. M. Hewett, E. J. Bocage, C. D. Winker, and B. J. O'Neill, 2002, Genetic stratigraphy, stratigraphic architecture, and reservoir stacking patterns of the Upper Miocene–Lower Pliocene Greater Mars-Ursa intraslope basin, Mississippi Canyon, Gulf of Mexico, *in* J. M. Armentrout and N. C. Rosen, eds., Sequence stratigraphic models for exploration and production: Evolving methodologies, emerging models, and application histories: Gulf Coast Section of the SEPM Foundation 22nd Annual Bob F. Perkins-Research Conference, Houston, Texas, December 8–11, 2002, p. 113–147.
Merrill, M. D., 2016, Geologic assessment of undiscovered conventional oil and gas resources in the Albian Clastic and updip Albian Clastic Assessment Units, U.S. Gulf Coast Region: Reston, Virginia, US Geological Survey Open-File Report 2016-1026, 28 p.
Mount, V. S., S. J. Wilkins, B. Lindsey, T. Butaud, P. Gamwell, T. Fowler, C. Morris, H. Adiguna, and B. McDonald, 2019, Structural configuration and evolution of subsalt hydrocarbon traps adjacent to salt walls, Green Canyon, Gulf of Mexico, *in* C. Fiduk, ed., Salt tectonics, associated processes, and exploration potential: Revisited: 1989–2019: 37th Annual Gulf Coast Section of the SEPM Foundation Perkins-Rosen Research Conference, Houston, Texas, December 3–6, 2019, p. 347–356.
Norton, I. O., L. A. Lawver, and J. W. Snedden, 2016, Gulf of Mexico tectonic evolution from Mexico deformation to oceanic crust, *in* C. M. Lowery, J. W. Snedden, and N. C. Rosen, eds., Mesozoic of the Gulf Rim and beyond: New progress in science and exploration of the Gulf of Mexico Basin: 35th Annual Gulf Coast Section of the SEPM Foundation Perkins-Rosen Research Conference, p. 1–12, doi:10.5724/gcs.15.35.0001.
Oehler, J. H., 1984, Carbonate source rocks in the Jurassic Smackover trend of Mississippi, Alabama, and Florida, *in* J. G. Palacas, ed., Petroleum geochemistry and source rock potential of carbonate rocks: AAPG Studies in Geology 18, p. 63–69.
Palacas, J. G., D. E. Anders, and J. D. King, 1984, South Florida basin—A prime example of carbonate source rocks of petroleum, *in* J. G. Palacas, ed., Petroleum geochemistry and source rock potential of carbonate rocks: AAPG Studies in Geology 18, p. 71–96.
Peel, F. J., 2019, Paleo-oceanographic preconditioning promotes precipitation: How the global context is a key factor for understanding Bajocian Louann Salt deposition,

in C. Fiduk, ed., Salt tectonics, associated processes, and exploration potential: Revisited: 1989–2019: 37th Annual Gulf Coast Section of the SEPM Foundation Perkins-Rosen Research Conference, Houston, Texas, December 3–6, 2019, p. 89–99.

Pepper, A. S., 2016, Back to the rocks: Framework of depositional acmes in source rocks of the Gulf of Mexico Basin and North Caribbean Margin: Gulf Coast Association of Geological Societies Transactions, v. 66, p. 853–858.

Peters, K. E., C. C. Walters, and J. M. Moldowan, 2007, The biomarker guide: Biomarkers and isotopes in petroleum exploration and Earth history: Cambridge, United Kingdom, Cambridge University Press, v. 2, 1155 p.

Petty, A. J., 1999, Petroleum exploration and stratigraphy of the Lower Cretaceous James Limestone (Aptian) and Andrew Formation (Albian): Main Pass, Viosca Knoll, and Mobile areas, northeastern Gulf of Mexico: Gulf Coast Association of Geological Societies Transactions, v. 49, p. 440–450.

Phelps, R. M., C. Kerans, R. O. B. P. Da-Gama, J. Jeremiah, D. Hull, and R. G. Loucks, 2015, Response and recovery of the Comanche carbonate platform surrounding multiple Cretaceous oceanic anoxic events, northern Gulf of Mexico: Cretaceous Research, v. 54, p. 117–144, doi:10.1016/j.cretres.2014.09.002.

Pilcher, R. S., B. Kilsdonk, and J. Trude, 2011, Primary basins and their boundaries in the deep-water northern Gulf of Mexico: Origin, trap types, and petroleum system implication: AAPG Bulletin, v. 95, no. 2, p. 219–240, doi:10.1306/06301010004.

Pilcher, R. S., R. T. Murphy, and J. M. Ciosek, 2014, Jurassic raft tectonics in the northeastern Gulf of Mexico: Interpretation, v. 2, no. 4, p. SM39–SM55, doi:10.1190/INT-2014-0058.1.

Pitman, J. K., R. F. Dubiel, P. H. Nelson, J. Kibler, R. R. Charpentier, T. A. Cook, T. R. Klett, R. Pollastro, and C. J. Schenk, 2007, Assessment of undiscovered gas resources in the Upper Cretaceous Tuscaloosa and Woodbine Formations, Western Gulf Province of the Gulf Coast region, Louisiana and Texas: Reston, Virginia, US Geological Survey Fact Sheet 2006-3146, 2 p.

Prather, B. E., J. R. Booth, G. S. Steffens, and P. A. Craig, 1998, Classification, lithologic calibration, and stratigraphic succession of the seismic facies of intraslope basins, deep-water Gulf of Mexico: AAPG Bulletin, v. 82, no. 5, p. 701–728.

Rowan, M. G., K. A. Giles, T. E. Hearon IV, and J. C. Fiduk, 2016, Megaflaps adjacent to salt diapirs: AAPG Bulletin, v. 100, no. 11, p. 1723–1747, doi:10.1306/05241616009.

Sanford, J. C., J. W. Snedden, and S. P. S. Gulick, 2016, The Cretaceous-Paleogene boundary deposit in the Gulf of Mexico: Large-scale oceanic basin response to the Chicxulub impact: Journal of Geophysical Research: Solid Earth, v. 121, no. 3, p. 1240–1261, doi:10.1002/2015JB012615.

Santamaria Orozco, D. M., 2000, Organic geochemistry of Tithonian source rocks and associated oils from the Sonda de Campeche, Mexico, Ph.D. dissertation, Rhine-Westphalia Institute of Technology, Aachen, Germany, 201 p.

Sassen, R., 1988, Geochemical and carbon isotopic studies of crude oil destruction, bitumen precipitation, and sulfate reduction in the deep Smackover Formation: Organic Geochemistry, v. 12, no. 4, p. 351–361, doi:10.1016/0146-6380(88)90009-5.

Sassen, R., 1990, Geochemistry of carbonate source rocks and crude oils in Jurassic salt basins of the Gulf Coast, *in* J. Brooks, ed., Classic petroleum provinces: Geological Society, London, Special Publications 1990, v. 50, p. 265–277, doi:10.1144/GSL.SP.1990.050.01.13.

Sassen, R., C. H. Moore, and F. C. Meendsen, 1987, Distribution of hydrocarbon source potential in the Jurassic Smackover Formation: Organic Geochemistry, v. 11, no. 5, p. 379–383, doi:10.1016/0146-6380(87)90070-2.

Schenk, C. J., 2008, Jurassic–Cretaceous composite total petroleum system and geologic models for oil and gas assessment of the North Cuba Basin, Cuba: Reston, Virginia, US Geological Survey Digital Data Series 69-M, 94 p.

Schlanger, S. O., and H. C. Jenkyns, 1976, Cretaceous oceanic anoxic events: Causes and consequences: Netherlands Journal of Geosciences, v. 55, p. 179–184.

Schowalter, T. T., 1979, Mechanics of secondary hydrocarbon migration and entrapment: AAPG Bulletin, v. 63, no. 5, p. 723–760.

Scott, R. W., N. Rush, R. Hojnacki, W. Campbell, Y. Wang, and X. Lai, 2020, Albian (Lower Cretaceous) carbon isotope chemozones, Texas Comanche Shelf and Mexican Chihuahua Trough: Implications for OAEs: Cretaceous Research, v. 112, 104453, doi:10.1016/j.cretres.2020.104453.

Seldon, B., and P. B. Flemings, 2005, Reservoir pressure and seafloor venting: Predicting trap integrity in a Gulf of Mexico deepwater turbidite minibasin: AAPG Bulletin, v. 89, no. 2, p. 193–209.

Smith, D. J., 2018, Success and failure in the deepwater Norphlet play, United States Gulf of Mexico: Gulf Coast Association of Geological Societies Transactions, v. 68, p. 635–642.

Smith, T., 2013, Unleasing the mad dog: GeoExPro, v. 10, no. 2, p. 22–27.

Snedden, J. W., 2013, Channel-body basal scours: Observations from 3D seismic and importance for subsurface reservoir connectivity: Marine and Petroleum Geology, v. 39, no. 1, p. 150–163, doi:10.1016/j.marpetgeo.2012.08.013.

Snedden, J. W., 2014, Estimating effective shale area distributions from subsurface data: Marine and Petroleum Geology, v. 49, p. 35–44, doi:10.1016/j.marpetgeo.2013.09.006.

Snedden, J. W., and W. E. Galloway, 2019, The Gulf of Mexico sedimentary basin: Depositional evolution and practical applications: Cambridge, United Kingdom, Cambridge University Press, 344 p., doi:10.1017/9781108292795.

Snedden, J. W., W. E. Galloway, K. T. Milliken, J. Xu, T. Whiteaker, and M. D. Blum, 2018, Validation of empirical source-to-sink scaling relationships in a continental-scale

system: The Gulf of Mexico basin Cenozoic record: Geosphere, v. 14, no. 2, p. 768–784, doi:10.1130/GES01452.1.

Snedden, J. W., I. O. Norton, M. R. Hudec, and F. Peel, 2019, Paleogeographic reconstruction of the Louann Salt Basin, *in* C. Fiduk, ed., Salt tectonics, associated processes, and exploration potential: Revisited: 1989–2019: 37th Annual Gulf Coast Section of the SEPM Foundation Perkins-Rosen Research Conference, Houston, Texas, December 3–6, 2019, p. 24–27.

Snedden, J. W., D. F. Stockli, and I. O. Norton, 2020, Palaeogeographical reconstruction and provenance of Oxfordian aeolian sandstone reservoirs in Mexico offshore areas: Comparison to the Norphlet aeolian system of the northern Gulf of Mexico, *in* I. Davison, J. N. F. Hull, and J. Pindell, eds., The basins, orogens and evolution of the southern Gulf of Mexico and northern Caribbean: Geological Society, London, Special Publications 2020, v. 504, 21 p., doi:10.1144/SP504-2019-219.

Snedden, J. W., J. Virdell, T. L. Whiteaker, and P. Ganey-Curry, 2016, A basin-scale perspective on Cenomanian-Turonian (Cretaceous) depositional systems, greater Gulf of Mexico (USA): Interpretation, v. 4, no. 1, p. SC1–SC22, doi:10.1190/INT-2015-0082.1.

Sneider, R. M., J. S. Sneider, G. W. Bolger, and J. W. Neasham, 1997, Comparison of seal capacity determinations: Conventional cores vs. cuttings, *in* R. C. Surdam, ed., Seals, traps, and the petroleum system: AAPG Memoir 67, p. 1–12.

Sternbach, C. A., 2020, What is the state of understanding of super basins, the world's richest oil and gas basins?: AAPG Search and Discovery article 70401, accessed October 4, 2020, http://www.searchanddiscovery.com/documents/2020/70401sternbach/ndx_sternbach.pdf.

Sullivan, M. D., J. L. Foreman, D. C. Jennette, D. Stern, G. N. Jensen, and F. J. Goulding, 2004, An integrated approach to characterization and modeling of deep-water reservoirs, Diana field, western Gulf of Mexico, *in* G. M. Grammer, P. M. Harris, and G. P. Eberli, eds., Integration of outcrop and modern analogs in reservoir modeling: AAPG Memoir 80, p. 215–234.

Sun, X., and R. Forkner, 2019, Geochemical and biomarker evidence of microbial community changes during Lower Cretaceous OAE 1b: Comanche Shelf, Glen Rose Formation, Central Texas (abs.): AAPG Annual Convention and Exhibition, San Antonio, Texas, May 19–22, 2019, accessed October 5, 2020, http://www.searchanddiscovery.com/abstracts/html/2019/ace2019/abstracts/2254.html.

Swanson, S. M., C. B. Enomoto, K. O. Dennen, B. J. Valentine, and C. D. Lohr, 2013a, Geologic assessment of undiscovered hydrocarbons in Lower to Upper Cretaceous carbonate rocks of the Fredericksburg and Washita groups, U.S. Gulf Coast Region: Gulf Coast Association of Geological Societies Transactions, v. 63, p. 423–437.

Swanson, S. M., A. W. Karlsen, and B. J. Valentine, 2013b, Geologic assessment of undiscovered oil and gas resources: Oligocene Frio and Anahuac Formations, United States Gulf of Mexico coastal plain and State waters: Reston, Virginia, US Geological Survey Open-File Report 2013-1257, 78 p., doi:10.3133/ofr20131257.

Sweet, M. L., and M. D. Blum, 2011, Paleocene-Eocene Wilcox submarine canyons and thick deepwater sands of the Gulf of Mexico: Very large systems in a greenhouse world, not a Messinian-like crisis: Gulf Coast Association of Geological Societies Transactions, v. 61, p. 443–450.

Sweet, M. L., and M. D. Blum, 2016, Connections between fluvial to shallow marine environments and submarine canyons: Implications for sediment transfer to deep water: Journal of Sedimentary Research, v. 86, no. 10, p. 1147–1162, doi:10.2110/jsr.2016.64.

Sweet, M. L., and L. T. Sumpter, 2007, Genesis field, Gulf of Mexico: Recognizing reservoir compartments on geologic and production time scales in deep-water reservoirs: AAPG Bulletin, v. 91, no. 12, p. 1701–1729, doi:10.1306/07190707011.

Syrio, J. C., P. S. da Cruz, N. V. Nguyen, A. Navarro, M. Becker, E. A. Watkins, L. A. Riera, and R. Leite, 2013, Cascade and Chinook fields: Integrated overview of the reservoirs: Offshore Technology Conference, Houston, Texas, May 6–9, 2013, OTC-24163-MS, 10 p., doi:10.4043/24163-MS.

Thacher, C., J. Stefani, C. Wu, K. Nihei, L. Sydora, T. Chou, L. Zhang, D. Bevc, B. Regel, and E. Clark, 2013, Subsalt imaging and 4D reservoir monitoring evaluation of Tahiti field, Gulf of Mexico: Society of Exploration Geophysicists Technical Program Expanded Abstracts 2013, Houston, Texas, September 22–27, 2013, p. 4875–4879, doi:10.1190/segam2013-1003.1.

Tsikos, H., H. C. Jenkyns, B. Walsworth-Bell, M. R. Petrizzo, A. Forster, S. Kolonic, E. Erba, et al., 2004a, Carbon-isotope stratigraphy recorded by the Cenomanian–Turonian oceanic anoxic event: Correlation and implications based on three key localities: Journal of the Geological Society, v. 161, no. 4, p. 711–719, doi:10.1144/0016-764903-077.

Tsikos, H., H. C. Jenkyns, B. Walsworth-Bell, M. R. Petrizzo, A. Forster, S. Kolonic, E. Erba, et al., 2004b, Erratum to Carbon-isotope stratigraphy recorded by the Cenomanian–Turonian oceanic anoxic event: Correlation and implications based on three key localities: Journal of the Geological Society, v. 162, no. 3, p. 576, doi:10.1144/0016-7649Er161-4.

Umbarger, K. F., 2018, Late Triassic North American paleodrainage networks and sediment dispersal of the Chinle Formation: A quantitative approach utilizing detrital zircons, Master's thesis, University of Kansas, Lawrence, Kansas, 131 p.

US Geological Survey, 2005, Assessment of undiscovered oil and gas resources of the North Cuba Basin, Cuba, 2004: Reston, Virginia, US Geological Survey World Assessment of Oil and Gas Fact Sheet 2005-3009, 2 p., accessed October 4, 2020, https://pubs.usgs.gov/fs/2005/3009/pdf/fs2005_3009.pdf.

Wardlaw, N. C., and R. P. Taylor, 1976, Mercury capillary pressure curves and the interpretation of pore structure and capillary behavior in reservoir rocks: Bulletin of Canadian Petroleum Geology, v. 24, no. 2, p. 225–262.

Weimer, P., R. Bouroullec, J. Adson, and S. P. J. Cossey, 2017a, An overview of the petroleum systems of the northern deep-water Gulf of Mexico: AAPG Bulletin, v. 101, no. 7, p. 941–993, doi:10.1306/09011608136.

Weimer, P., R. Bouroullec, V. Matt, J. Adson, A. A. van den Berg, T. G. Lapinski, and J. G. Roesink, 2016a, Petroleum geology of the Mississippi Canyon, Atwater Valley, western DeSoto Canyon, and western Lloyd protraction areas, northern deepwater Gulf of Mexico: Seals, source rocks, generation, and accumulation: Preliminary results: Gulf Coast Association of Geological Societies Transactions, v. 66, p. 601–624.

Weimer, P., R. Bouroullec, and O. Serrano, 2017b, Petroleum geology of the Mississippi Canyon, Atwater Valley, western DeSoto Canyon, and western Lloyd Ridge protraction areas, northern deep-water Gulf of Mexico: Traps, reservoirs, and tectono-stratigraphic evolution: AAPG Bulletin, v. 101, no. 7, p. 1073–1108, doi:10.1306/09011610093.

Weimer, P., R. Bouroullec, A. A. van den Berg, T. G. Lapinski, J. G. Roesink, and J. Adson, 2017c, Structural setting and evolution of the Mensa and Thunder Horse intraslope basins, northern deep-water Gulf of Mexico: A case study: AAPG Bulletin, v. 101, no. 7, p. 1145–1172, doi:10.1306/09011609112.

Weimer, P., R. Bouroullec, E. Zimmermann, H. Pettingill, and W. Gutterman, 2016b, Temporal and spatial evolution of traps, northern deepwater Gulf of Mexico: Gulf Coast Association of Geological Societies Transactions, v. 66, p. 557–567.

Weimer, P., J. R. Crews, R. S. Crow, and P. Varnai, 1998, Atlas of petroleum fields and discoveries, northern Green Canyon, Ewing Bank, and offshore southern Ship Shoal and South Timbalier areas (offshore Louisiana), northern Gulf of Mexico: AAPG Bulletin, v. 82, no. 5, p. 878–917.

Wenger, L. M., L. R. Goodoff, O. P. Gross, S. C. Harrison, and K. C. Hood, 1994, Northern Gulf of Mexico: An integrated approach to source, maturation, and migration, *in* N. Scheidermann, P. Cruz, and R. Sanchez, eds., Geologic aspects of petroleum systems: 1st Joint AAPG/Association of Mexican Petroleum Geologists Hedberg Research Conference, Mexico City, Mexico, October 2–6, 1994, 5 p.

Wilkins, S., V. Mount, R. Davies, T. Butaud, B. Lindsey, C. Fenn, J. Syrek, H. Adiguna, and I. Matthews, 2019, Sub-seismic deformation in traps adjacent to salt stocks/walls: Observations from Green Canyon, Gulf of Mexico: European Association of Geoscientists & Engineers Fifth International Conference on Fault and Top Seals, Palermo, Italy, September 9–12, 2019, 5 p., doi:10.3997/2214-4609.201902288.

Yurewicz, D. A., R. J. Chuchla, M. Richardson, R. J. Pottorf, G. G. Gray, M. G. Kozar, and W. M. Fitchen, 1997, Hydrocarbon generation and migration in the Tampico–Misantla Basin and Sierra Madre Oriental, east-central Mexico: Evidence from an exhumed oil field in the Sierra de el Abra, *in* P. Enos, R. R. Aracen, C. J. Minero, and D. Yurewicz, eds., Sedimentation and diagenesis of Middle Cretaceous platform margins, east central Mexico: AAPG Field Trip Guidebook 4, 24 p.

Zarra, L., 2007, Chronostratigraphic framework for the Wilcox Formation (Upper Paleocene–Lower Eocene) in the deepwater Gulf of Mexico: Biostratigraphy, sequences, and depositional systems, *in* L. Kennan, J. Pindell, and N. C. Rosen, eds., The Paleogene of the Gulf of Mexico and Caribbean Basins: Processes, events and petroleum systems: 27th Annual Gulf Coast Section of the SEPM Foundation Bob F. Perkins Research Conference, Houston, Texas, December 2–5, 2007, p. 81–146. doi:10.5724/gcs.07.27.0081.

Zarra, L., R. Hackworth, and A. Kahn, 2019, Wilcox chronostratigraphic framework update: AAPG Search and Discovery article 51616, accessed October 4, 2020, http://www.searchanddiscovery.com/documents/2019/51616zarra/ndx_zarra.pdf.

Zumberge, J., H. Illich, and L. Waite, 2016, Petroleum geochemistry of the Cenomanian–Turonian Eagle Ford oils of south Texas, *in* J. Breyer, ed., The Eagle Ford Shale: A renaissance in U.S. oil production: AAPG Memoir 110, p. 135–165, doi:10.1306/13541960M110449.